Carderock Division
**Naval Surface Warfare Center**
West Bethesda, Maryland 20817-5700

NSWCCD-50-TR-2010/051 August, 2010
Hydromechanics Department Report

# Measurement of Steady and Unsteady Duct Loads for Propeller 4381 at Crashback Conditions in the 36" Water Tunnel

by

Martin J. Donnelly
Stuart Jessup
Ali Etebari





NSWCCD-50-TR-2010/051 Measurement of Steady and Unsteady Duct Loads for Propeller 4381 at Crashback Conditions in the 36" Water Tunnel

# REPORT DOCUMENTATION PAGE

*Form Approved*
*OMB No. 0704-0188*



| 1. AGENCY USE ONLY (Leave blank) | 2. REPORT DATE | 3. REPORT TYPE AND DATES COVERED |
|---|---|---|
| | August 2010 | Final |

**4. TITLE AND SUBTITLE**

Measurement of Steady and Unsteady Duct Loads for Propeller 4381 at Crashback conditions in the 36" Water Tunnel

**5. FUNDING NUMBERS**

WX20739/AA
WX20696/AA

**6. AUTHOR(S)**

Martin J. Donnelly, Stuart Jessup, Ali Etebari

**7. PERFORMING ORGANIZATION NAME(S) AND ADDRESS(ES)**

Carderock Division, Naval Surface Warfare Center
Resistance and Propulsion, Code 5800
9500 MacArthur Boulevard
West Bethesda, Maryland 20817-5700

**8. PERFORMING ORGANIZATION REPORT NUMBER**

NSWCCD-50-TR-2010/051

**9. SPONSORING / MONITORING AGENCY NAME(S) AND ADDRESS(ES)**

Dr. Ki-Han Kim
Office of Naval Research
One Liberty Center
875 North Randolph Street, Suite 1425
Arlington, VA 22203-1995
(703) 588-2363

**10. SPONSORING / MONITORING AGENCY REPORT NUMBER**

**11. SUPPLEMENTARY NOTES**

**12a. DISTRIBUTION / AVAILABILITY STATEMENT**

Approved for public release: distribution unlimited.

**12b. DISTRIBUTION CODE**

**13. ABSTRACT** *(Maximum 200 words)*

*Unsteady forces and moments were measured on a generic ducted propeller (P4381) under simulated crashback conditions in the 36 inch variable pressure water tunnel at the Naval Surface Warfare Center, Carderock Division. Both rotor and duct forces were measured using 6-component dynamometers in order to determine total propulsor forces. The duct forces were found to be responsible for the majority of the side force, exceeding the propeller side force by as much as three times. Little difference was noted between the vector sum of the rotor and stator force components due to phasing between the two components and the dominant forcing frequencies present in the signal. The unsteady rotor side forces were noted to be approximately 10% of the mean propulsor thrust, while the total side force (rotor plus stator) is approximately 30% of the rotor thrust.*

| 14. SUBJECT TERMS | 15. NUMBER OF PAGES |
|---|---|
| Propeller 4381, CFD validation, crashback, ducted propeller, side forces, unsteady forces | 37 + iv |
| | 16. PRICE CODE |

| 17. SECURITY CLASSIFICATION OF REPORT | 18. SECURITY CLASSIFICATION OF THIS PAGE | 19. SECURITY CLASSIFICATION OF ABSTRACT | 20. LIMITATION OF ABSTRACT |
|---|---|---|---|
| Unclassified | Unclassified | Unclassified | Unclassified |

NSN 7540-01-280-5500 Standard Form 298 (Rev. 2-89)

THIS PAGE INTENTIONALLY LEFT BLANK

# Contents

## Figures

## NOMENCLATURE and ABBREVIATIONS

| | |
|---|---|
| 6DOF | six Degrees Of Freedom |
| CFD | Computational Fluid Dynamics |
| DTMB | David Taylor Model Basin |
| LDV | Laser Doppler Veloeimetry |
| LES | Large-Eddy Simulation |
| NAVSEA | Naval Sea Systems Command |
| NI | National Instruments |
| NSWCCD | Naval Surface Warfare Center, Carderoek Division |
| ONR | Office of Naval Research |
| PIV | Partiele Image Veloeimetry |
| RANS | Reynolds-averaged Navier-Stokes |
| SLA | Stereo Lithography Apparatus |
| SPIV | Stereo Partiele Image Veloeimetry |
| 36inWT | 36 ineh Water Tunnel |
| D | propellcr diameter |
| J | advance coefficient, U/nD |
| FV | vertieal Side force in inertial frame at TDC, $\theta = 0$ |
| FH | horizontal side force in inertial frame at TDC, $\theta = 0$ |
| Fx | horizontal side force in rotating frame |
| Fy | vertieal side force in rotating frame |
| FMAG | veetor sum of FV and FH |
| $K_T$ | thrust coefficient, $T/\rho n^2 D^4$ |
| $K_Q$ | torque coefficient, $Q/\rho n^2 D^5$ |
| Q | propeller torque |
| T | propeller thrust |
| U | water tunnel veloeity |
| n | propeller rotation rate, rps |
| P | blade piteh |
| $p_0$ | tunnel static pressure |
| $\rho$ | water density |
| $\theta$ | angular position, 0 at TDC |
| $\omega$ | propeller angular veloeity |

THIS PAGE INTENTIONALLY LEFT BLANK

## ABSTRACT

Unsteady forces and moments were measured on a generic ducted propeller (P4381) under simulated crashback conditions in the 36 inch variable pressure water tunnel at the Naval Surface Warfare Center, Carderock Division. Both rotor and duct forces were measured using 6-component dynamometers in order to determine total propulsor forces. The duct forces were found to be responsible for the majority of the side force, exceeding the rotor side force by as much as three times. Little difference was noted between the vector sum of the rotor and stator force components due to phasing between the two components and the dominant forcing frequencies present in the signal. The unsteady rotor side forces were noted to be approximately 10% of the mean propulsor (rotor plus stator) thrust, while the total side force (rotor plus stator) is approximately 30% of the rotor thrust.



## ADMINISTRATIVE INFORMATION

This work was performed at the Naval Surface Warfare Center, Carderock Division, West Bethesda, MD 20817 and was sponsored by the Office of Naval Research under the direction of Dr. Ki-Han Kim. The Project Leader is Dr. Stuart Jessup Senior Scientist for Hydro Mechanics, (Code 5030). Work was performed under work unit numbers 07-1-5030-101, and 08-1-5030-101, sponsor order number WX20739/AA and WX20696/AA.


## INTRODUCTION

From a propulsion standpoint, accurate prediction of the magnitude of loads experienced by propeller blades under various operational conditions is necessary to guide design and maintenance. While propeller performance can be accurately predicted at near-design conditions, off-design conditions pose significant challenges. Typically, potential flow codes are used to predict these phenomena, and prove sufficient under simple, steady conditions. Namely, these are the ahead (forward) or astern (backing) conditions. For the two propeller operational modes for which the ship velocity, $V_s$, opposes the propeller angular velocity, $\omega$, the flow becomes vastly more complex due to the shear layer interaction between the free stream and the flow exiting the propeller. These are known as the crashback ($+V_s$, $-\omega$) and crashahead ($-V_s$, $+\omega$) conditions. Crashback is an off-design propeller operational condition in which the propeller rotates in a backing mode, decelerating the vessel as it moves forward. The interaction of the free stream and opposing jet flow exiting the propeller generates a ring vortex that oscillates near the propeller tip. This unsteady flow induces side forces on the propeller that can greatly exceed the forces observed under normal operational conditions. These loads often control the structural criteria for propeller design. Furthermore, they can be large in comparison to the restoring or maneuvering forces on the control surfaces, resulting in uncontrolled lateral motions. This is in large part due to the fact that the control authority diminishes with decreasing speed in a crashback condition while propeller forces depend on both speed of advance and propeller rotational speed.

The primary objectives of this test are to measure both the rotor and duct/stator loads on a ducted propeller, and to determine the impact on side force magnitudes and rotational

frequencies due to the presence of a duct. The overall load split of side force magnitude will be determined as well. Propeller 4381 was selected for this study as a generic propeller that has been used previously in crashback studies, and can be used for Computation Fluid Dynamics (CFD) validation. The current testing program builds upon two previous testing efforts conducted in the 36inWT with propeller 4381. The first test conducted in 2004 was documented in Chesnakas et al (2004). In this test propeller 4381 was run as an open propeller in crashback,. Only shaft thrust and torque were measured along with Particle Image Velocimetry (PIV) measurements of local flow-fields at the blade leading edges and ring vortex flows. The second test conducted in 2005 is documented in Jessup et al (2006). During the second test period, the 4381 open propeller configuration was repeated with an in-hub 6-component dynamometer in order to measure out of plane or maneuvering forces. A neutrally loaded duct was also incorporated into the model setup. At this time the capability to measure duct/stator loads for this setup did not exist and only rotor forces were recorded. The primary test objective was to document the flow field changes as a result of the duct using PIV. The current test period addresses the missing data from that test with the inclusion of a new duct/stator load cell design. Rotor force data acquired previously with the duct will be compared to the current test data to insure consistency of the results.

## BACKGROUND

The crashback maneuver has been studied fairly extensively over the past decade. The first flow measurements were performed by Jiang (1), in which PIV measurements were used to relate flow features with measured unsteady shaft forces. This work revealed the presence of a ring vortex structure and its unsteadiness. In particular, the ring vortex was observed to undergo low frequency shedding unrelated to the propeller rotation rate. Later, Jessup (2) supported these findings with a comprehensive set of PIV and Laser Doppler Velocimetry (LDV) data. CFD efforts using Reynolds-averaged Navier-Stokes (RANS) include Chen (3) and Davoudzadeh (4). Chen (3) used RANS to simulate crashback on Propeller 4381. The computations over predicted the forces in comparison with experimental open water data, and only included modeling of a single blade passage, assuming blade periodic flow. It was concluded that cavitation was responsible for the discrepancy. Davoudzadeh (4) used RANS to simulate flow over the entire submarine body and propeller during crashback. An unsteady vortex ring was noted, but a comparison with experimental data was not provided. More recently, Vyoshlid and Mahesh (5, 6) modeled crashback loads using large eddy simulations (LES) for both a full propeller model of 4381 and an actuator disk model.

## EXPERIMENTAL SET-UP

### *Test facility*

The experiment was conducted in the Naval Surface Warfare Center Carderock Division's 36-inch Variable Pressure Cavitation Tunnel. The facility is a vertical plane, closed re-circulating tunnel with resorber, variable-speed, variable-pressure, two interchangeable circular test sections – an open jet and a closed jet, a deaerator, and a filter system (95-micron).

The drive system is made up of a 1.98 m diameter adjustable pitch four-bladed axial flow impeller, capable of a maximum test section velocity of 25.7 m/s and absolute pressures between 14 to 414 kPa. Specifications for the test facility are found in Appendix A.

Tunnel velocity measurements are determined from pressure drop using area ratios between static pressure tap locations. The 36in VPWT has 3 rings of taps for measurement of static pressure in the tunnel contraction upstream of the test section. Tunnel velocity is normally determined between Ring 3 and Ring 1 as they have the largest area difference and greatest pressure drop. Due to the reverse flow generated by a propeller in crashback the static pressure measurement at Ring 1, or closest to the test section, can include an unknown bias error. For this reason another measurement of velocity between Ring 3 and Ring 2 is also included in the data set. Advance coefficient values reported here use the velocity determined from Ring 3 to Ring 2.

### *Ducted configuration*

Propeller 4381 was tested during this effort. It is a five bladed propeller, 12 inches (304.8 mm) in diameter. A duct with supporting straight vanes was designed as a back-fit to propeller 4381 and constructed using a Stereo-Lithography Apparatus (SLA). Photographs of the test set-up are shown below in Figure 1. Detailed model characteristics for both the propeller and duct are given in Appendix B. Both the rotor (propeller shaft) and the stator/duct were instrumented with 6 component dynamometers. Drawings of the dynamometers are shown in Appendix C. The rotor cable was run through the shaft to a slip ring that allowed rotation of the dynamometer with the shaft. The stator cable was taped to the shaft, a strut, and back out through the tunnel wall using metal tape, as shown in Figure 2.

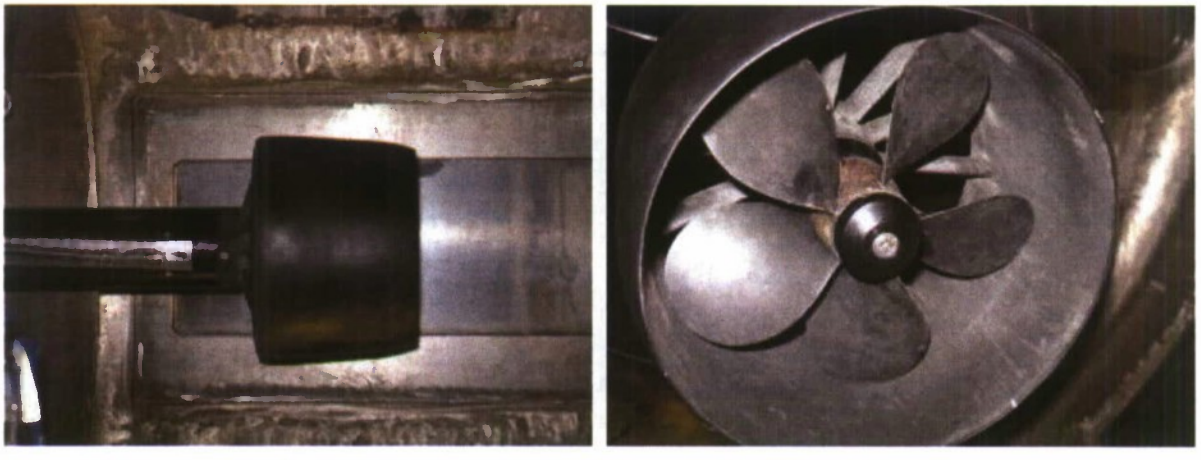

Figure 1. Ducted propeller 4381 configuration in the 36 inch water tunnel.

Figure 2. Shaft showing stator dynamometer cable faired to shaft, strut, and tunnel wall.

### *Data Acquisition System*

Measurements are taken with a Dell Optiplex GX270 running Windows 2000. Data acquisition software and analysis routines are written in LabVIEW v7.1. This collection and analysis code is called "36VPWT crashback rotor and duct.llb" and was developed within Code 5400. The PC utilizes a National Instruments PCI-6031E for analog measurements. The PCI-6031E is a 64 channel, 16 bit A/D with a maximum sampling rate of 100 kHz. In order to reduce system noise, the board is used in a differential mode limiting the number of analog inputs to 32. Physical connections to the data acquisition card are made through BNC blocks (NI part numbers BNC2110 and BNC2115). In order to correlate the measured analog data to shaft position the PCI-6031E is synchronized with a digital input board, PCI-DIO-32HS, through the Real Time System Integration (RTSI) bus. The PCI-DIO-32HS is connected to an absolute position encoder in order to record shaft position through a screw terminal connection block (NI part number SCB-68). All data were sampled at a rate of 500 Hz. Previous crashback testing efforts determined this sampling rate to be sufficient to resolve unsteady signals of interest.

Two AMTI 6-component dynamometers are used to measure rotor and stator forces and moments. Both dynamometers were calibrated for all 6 force and moment components prior to the experiment. The results for these calibration efforts are given in Appendix D: Rotor and stator dynamometer calibrations, with gains, sensitivity matrices, and calibration uncertainty included. The rotor dynamometer rotates with the shaft and also includes a force component corresponding to the weight of the propeller. For this reason these measurements are synchronized with the absolute position shaft encoder. This permits subtraction of the weight of the propeller from the side force measurements, and conversion of the side force measurements into the inertial frame. The process behind synchronizing the AMTI orientation with the absolute position shaft encoder and for subtracting the weight of the propeller are described later in the text.

# DATA REDUCTION

## *Data Acquisition Scheme*

By collecting six-component voltage data from the rotor dynamometer and the digital output from the absolute position encoder simultaneously, rotating forces and moments can be reduced into a body, fixed-frame coordinate system. Voltage data are multiplied by a sensitivity calibration and interaction matrix to derive engineering units, and 13-bits of digital data are summed to generate a value from 0-8192 indicating angular position. By implementing a high-speed digital interface, all 13 bits of encoder data can be sampled between transitions resulting in a noise free signal. This is critical to enable accurate transformation of the rotating data into an inertial reference frame. Data channels are sampled at 500 Hz, at a sweep rate of 1.25 MHz, resulting in a virtually simultaneous sampling rate. Both the dynamometers were sampled simultaneously. When summing the propeller and duct forces, this was done at the 500 Hz collection rate.

## *Coordinate System Conversion*

The coordinate system shown in Figure 3 was used for data acquisition and reduction. To resolve the measured rotating forces (FX rotor, FY rotor) into a body fixed coordinate system, encoder values aligned with body fixed axes ($\theta = 0$, 90, 180, and 270°) had to be determined. To do this a Zero Reference or Rotating Zero Procedure was established and repeated for several model setups to determine its accuracy.

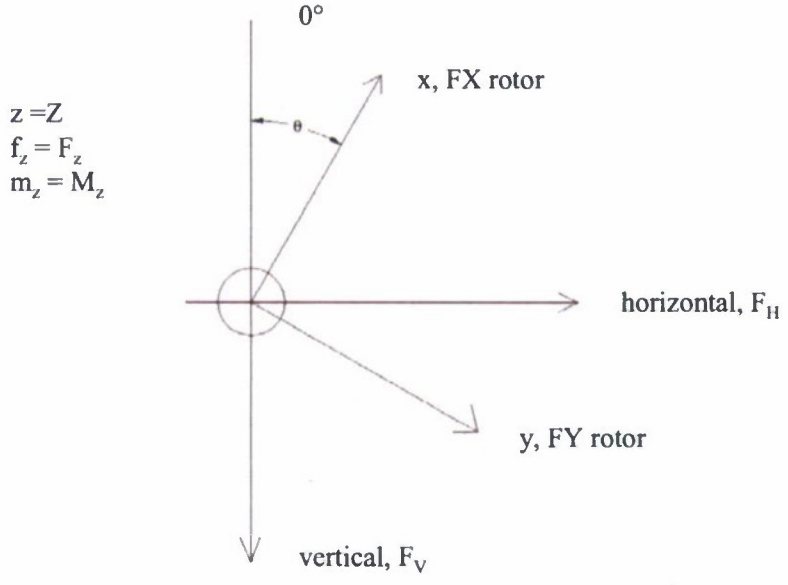


Figure 3. Coordinate System Looking Upstream.

### *Zero Reference or Rotating Zero Procedure*

The purpose of the zero reference or rotating zero procedure is twofold. The first is to determine the encoder locations aligned with the body fixed coordinate system and the second is to calculate a set of rotor weight functions. The rotor weight functions represent the measured forces on the propeller dynamometer for one complete revolution at no flow. Subtraction of the rotor weight functions from operating data at each angular location reveals the hydrodynamic forces acting on the propeller.

The dynamometer, with propeller installed, was rotated to a fixed angle and a 5-second average was taken of each channel. The shaft is then rotated to a new location and data is acquired. This process is repeated until data are collected at enough angular positions to define the rotor weight functions for one rotation of the propeller. The above procedure was also conducted with a dry test section to determine encoder reference locations, as it did not include buoyancy effects in the rotor weight functions or any shaft windup under load. Due to the low loading relative to the shafting size, this wind-up could be ignored.

This data is then curve fit using a curve fitting routine, NLREG v6.0. The rotor weight functions are listed below,

$$W_x = offset_x + weight \times \sin(theta - phi)$$
$$W_y = offsety + weight \times \cos(theta - phi)$$

The values $offset_x$ and $offset_y$ are a function of zeroing the dynamometer at an unknown angular location. These offsets are addressed in the electrical zeroes procedure below. Theta is the measured angular position of the shaft, and phi is the offset angle where dynamometer channel; Fx is vertical and Fy is horizontal to starboard. Weight represents the weight of the propeller. Raw data from this procedure is show in Figure 4. For this case $offset_x$ = -0.615 lbs, $offset_y$ = -0.0281 lbs, weight = 2.02 lbs, and phi = -0.178 degrees.

Even though the propeller weight is well known and could be represented by a shifted sinusoidal function it is best to determine these functions experimentally. The experimental fitting procedure takes into account all additional pieces hanging on the dynamometer (propeller, spacers, fairwater), the weight of the dynamometer itself, and accounts for buoyancy effects when conducted with the propeller submerged. The number of data points shown was representative of the angular increment required to accurately determine the propeller weight and phi offset angle.

To determine the encoder reference positions the Fx and Fy sinusoidal curve fits were examined to determine there maximum and minimum encoder locations. Where Fx is minimum, largest negative value, corresponds to 0°. This encoder location could then be subtracted from each encoder measurement so that the data are referenced to 0° at top dead center (TDC). Where Fx is maximum corresponds to 180°. Where Fy is maximum corresponds to Fx at 90°, and where Fy is minimum corresponds to Fx towards 270°. Repetition of this procedure both dry and wet and on subsequent days of testing showed at most a ± 1.0° error in calculated reference positions. The error can be largely attributed to the number of data points taken around each maximum and minimum encoder location. Figure 5 displays the FX and FY weight data with their respective curve fits after including voltage offsets and processing with the 6-component calibration and interaction matrix.

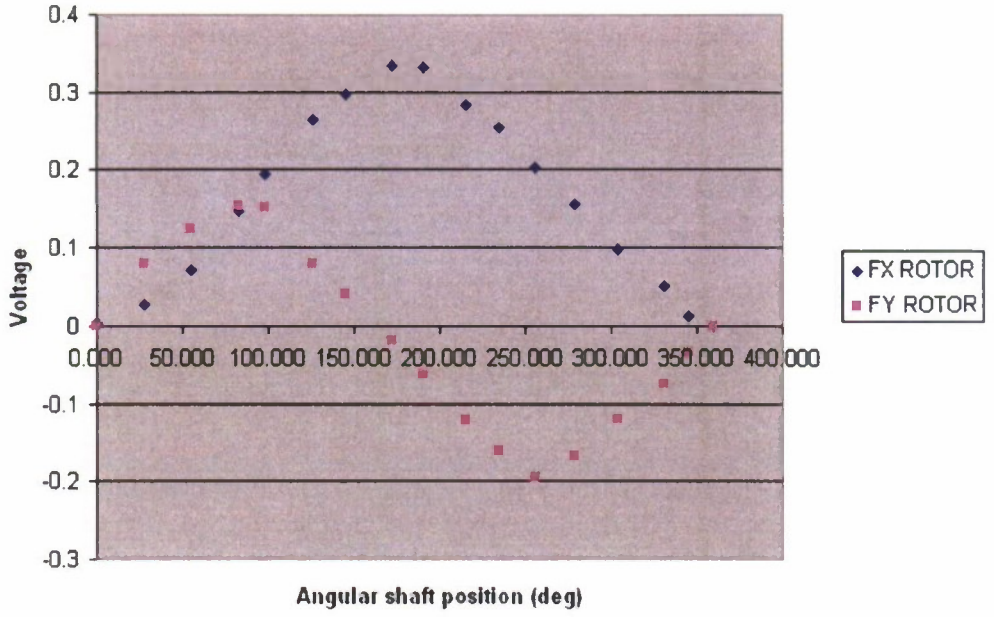


Figure 4. Raw Data from Rotor Weight Function.

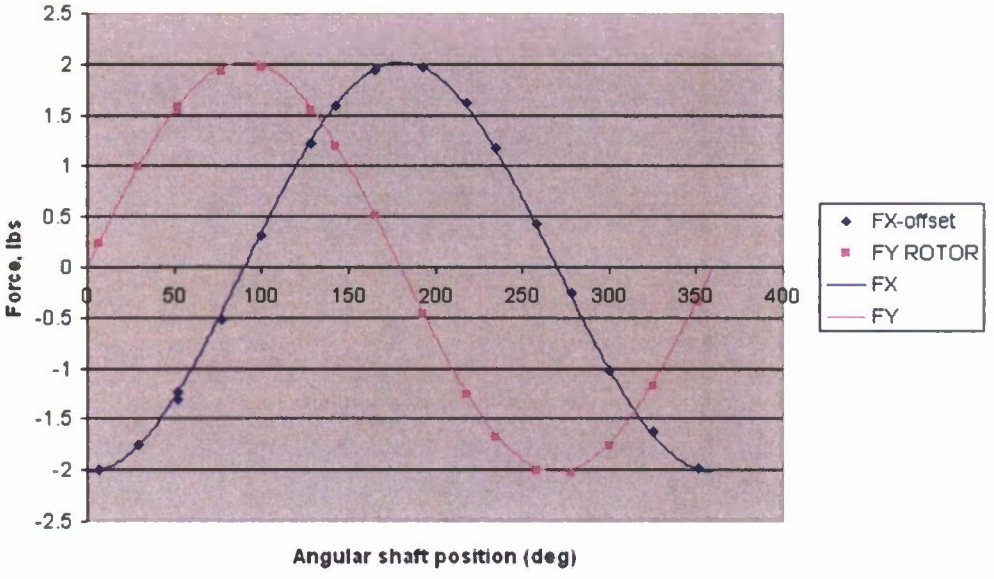


Figure 5. Data from Rotor Weight Function with curve fits.

### *Electrical Zeroes*

To set electrical zeroes the dynamometer is rotated by hand to the calculated encoder position at 0°. This is done by reading the encoder position and communicating with the tunnel operator rotating the shaft. At this position Fy and Mx should be equal to zero. Zeroing all of the channels simultaneously creates an offset equal to half the propeller weight on Fx and a corresponding moment offset on My. These offsets are added back into the measured data during the real-time data reduction algorithms. The offsets are also determined experimentally by repeating the zero reference procedure to verify the zero reference position.

### *Propeller Weight Subtraction*

With the propeller rotor weight functions determined under static conditions they can then be subtracted from dynamic measurements. This is accomplished by simultaneously measuring rotor forces and shaft position. Example data from unsteady runs are shown in Figures Figure 6 and Figure 7 below. These measurements were made during LCC crashback measurements discussed in Bridges (7) in which P4381 was mounted behind a submarine body. No unsteady runs, ramped rpm, or tunnel speed have been made for the 36inWT configuration. The portion of the data set where the rpm is positive corresponds to a forward rotation of the rotor. When the propeller weight is subtracted the portion is zeroed leaving only the hydrodynamic forces on the rotor.

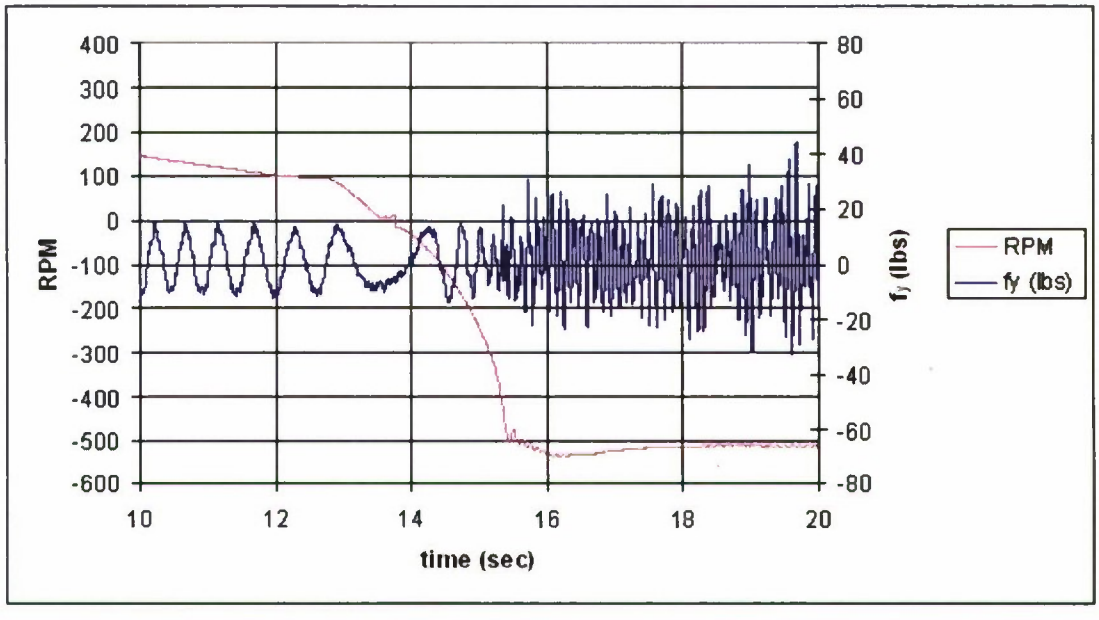


Figure 6. Ramped RPM and tunnel speed, rotating side force component (Fy).

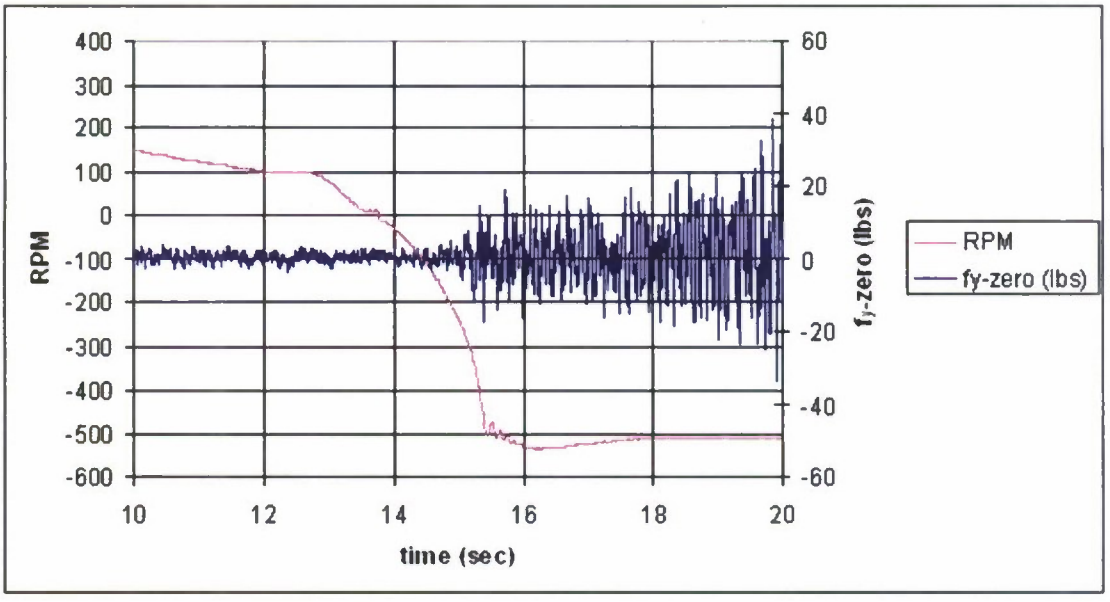


Figure 7. Ramped rpm and tunnel speed, rotating side force with propeller weight subtracted, (Fy-W).

### *Determine Forces in the Inertial Frame*

Rotor side forces FX rotor and FY rotor can be converted into an inertial or fixed frame of reference. The equations below represent the coordinate system shown in Figure 3.

$$FH_{rotor} = (FX - W)\sin\theta + (FY - W)\cos\theta$$
$$FV_{rotor} = (FX - W)\cos\theta - (FY - W)\sin\theta$$

The vector sum of these components is equal to the rotor side force magnitude.

$$FMAG_{rotor} = \sqrt{FH_{rotor}^{\ 2} + FV_{rotor}^{\ 2}}$$

The side force magnitude can be non-dimensionalized as a propeller force coefficient,

$$KFMAG_{rotor} = FMAG_{rotor} \Big/ (\rho n^2 D^4)$$

where , $\rho$ is the fluid density, $n$ is the rotational speed in rev/s of the propeller, and $D$ is the propeller diameter. The non-dimensional thrust coefficient, $K_T$, is given by

$$K_T = \frac{T}{\rho n^2 D^4}$$

where T is the thrust. The non-dimensional torque coefficient, $K_Q$, is given by

$$K_Q = \frac{Q}{\rho n^2 D^5}$$

where Q is the torque.

## RESULTS AND DISCUSSION

Figure 8 shows the non-dimensional rotor thrust and torque coefficients for the ducted and open configurations for crashback conditions. There is little difference between the rotor thrust or torque coefficients in either the ducted and open propeller configurations, although the ducted configuration shows a small increase in magnitude as $J$ approaches 0 in the crashback condition. The ducted thrust coefficient appears to be slightly higher than the open configuration, while the torque coefficient tends to be marginally higher for the open configuration than the ducted configuration. Figure 9 shows the non-dimensional rotor thrust and torque coefficients for the ducted and open configurations for ahead conditions. The ahead conditions show very little difference between the rotor thrust or torque coefficients in the ducted and open propeller configurations. Figure 10 shows the propeller side force, KFMAG, verses J for both crashback and ahead conditions. The previous rotor force only measurements with the duct, labeled "ducted (Chesnakas, 2005)" taken from Chesnakas (8), agrees with the present measurement, labeled "ducted (2008)". The open propeller case, without duct, also matched both ducted cases indicating that the presence of the duct does not impact the propeller side force loading. Figure 11 shows the propeller force coefficient, KFMAG, propeller and duct components for the ducted configuration. KFMAG for the duct is responsible for the majority of the total force. Furthermore, it is clear that the duct and rotor components are out of phase over most of the advance coefficients, as the sum of the two components does not equal the total KFMAG. Near the peak that shows up at an advance coefficient of -0.3, the two appear to be almost completely out of phase. The phase offset between the two reduces the peak magnitude of the total propeller force significantly. This observation is supported by Figure 12 and Figure 13, which display KT and KQ for the crashback conditions with the rotor, duct, and total components shown. To illustrate the phase offset between duct and propeller forces, the horizontal and vertical force components for J = -0.345 are shown in Figure 14 and Figure 15. It is clear from these figures that the duct force is responsible for most of the total force and that the signals are out of phase at this $J$ value. Both signals are dominated by a low frequency with a period of approximately three seconds.

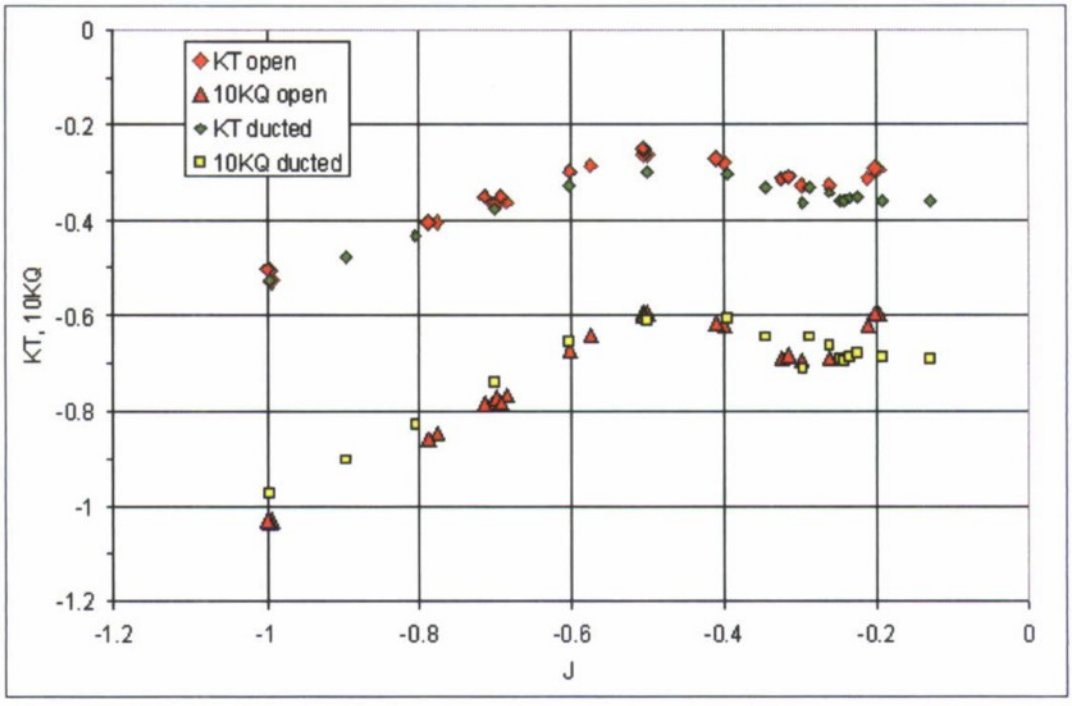


Figure 8. Rotor component of thrust coefficient (KT) and torque coefficient (KQ) for the open and ducted propeller configurations under simulated crashback conditions.

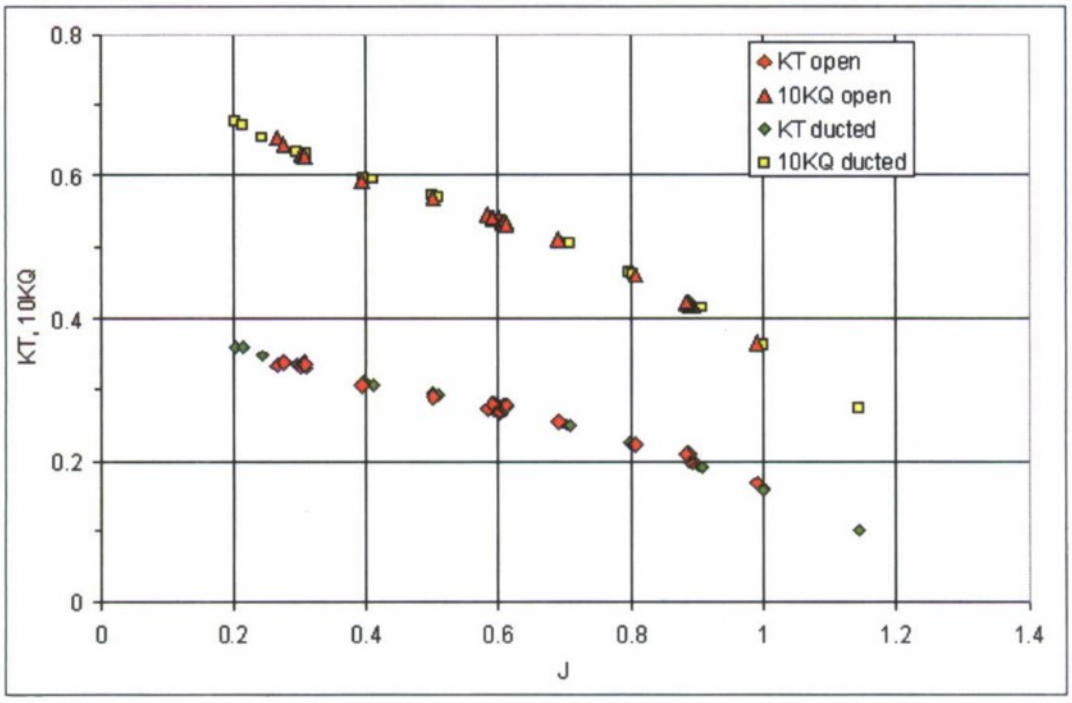


Figure 9. Rotor component of thrust coefficient (KT) and torque coefficient (KQ) for the open and ducted propeller configurations under ahead conditions.

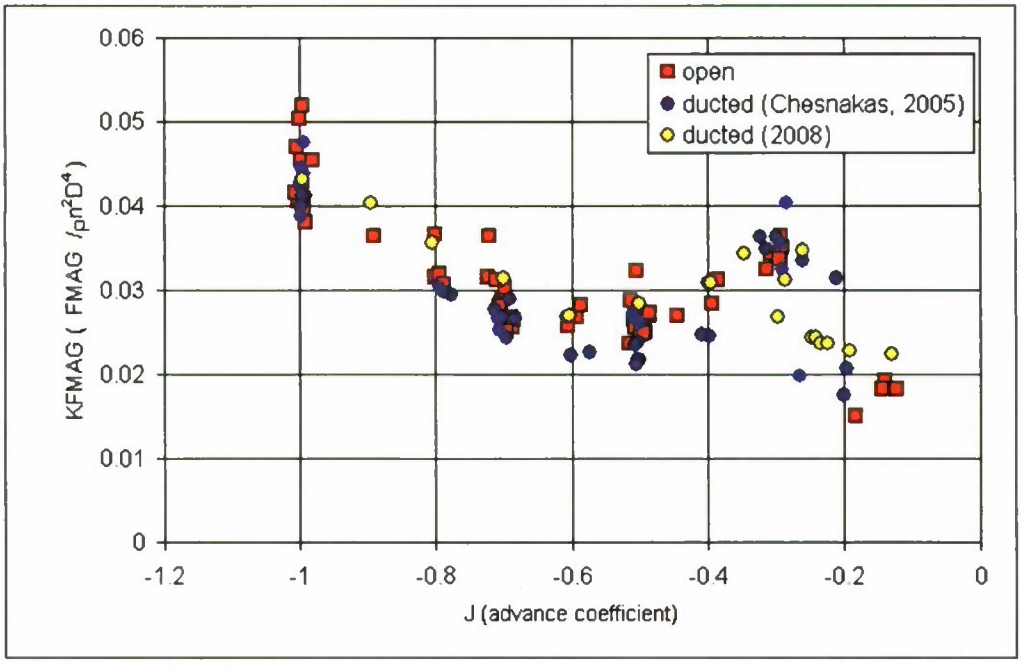


Figure 10. Propeller force coefficient (KFMAG) comparisons for the open and ducted propeller configurations under crashback conditions.

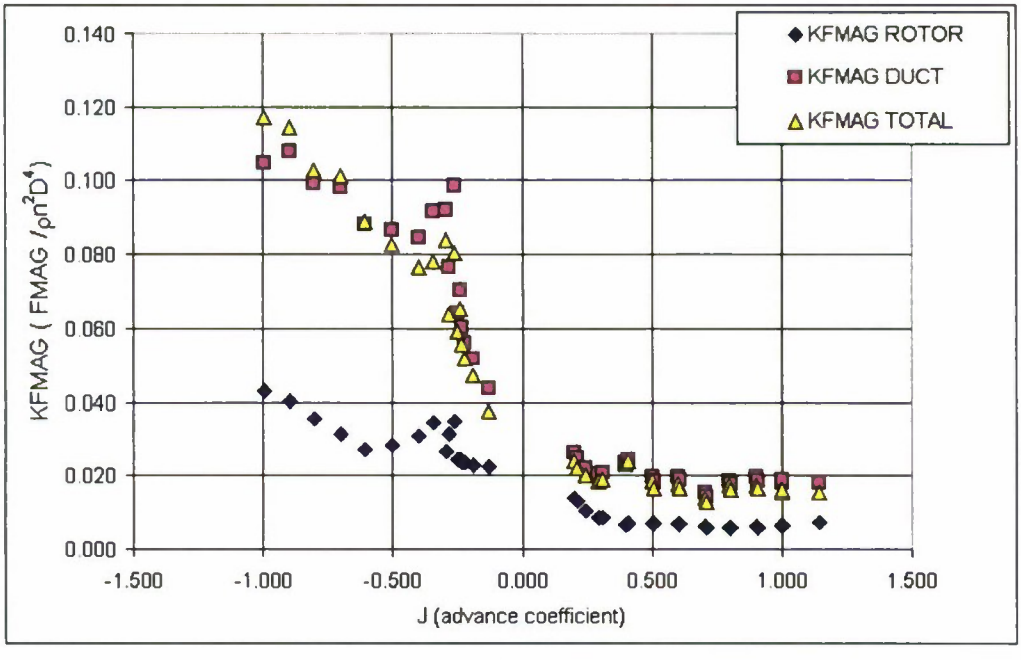


Figure 11. Propeller force coefficient (KFMAG) for rotor, duct, and combined magnitude for ducted propeller configuration under crashback conditions.

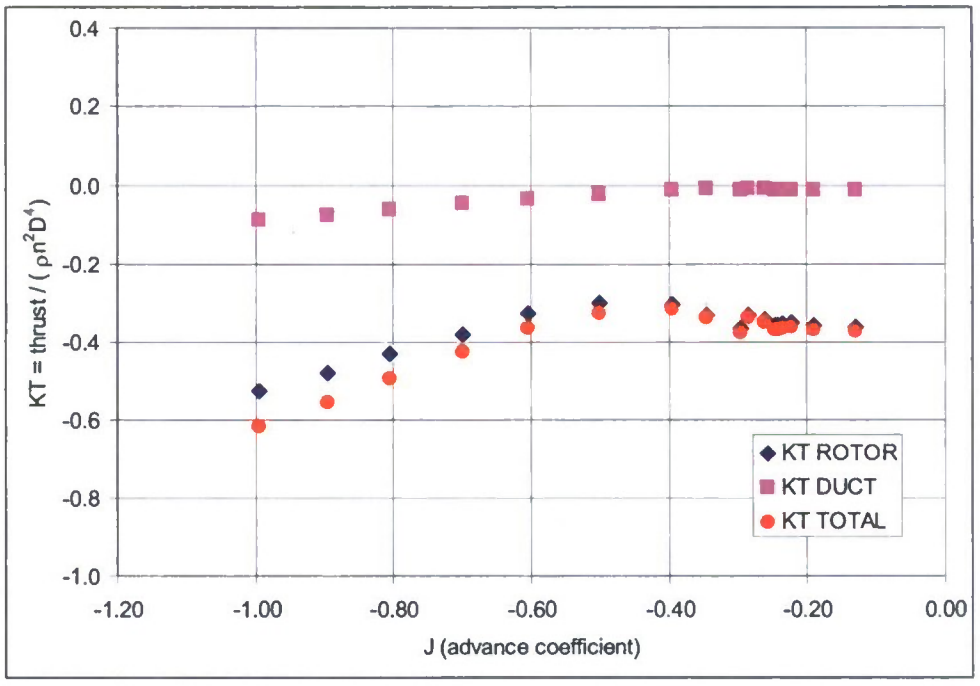


Figure 12. Propeller thrust coefficient (KT) for rotor, duct, and combined magnitude for ducted propeller configuration under crashback conditions.

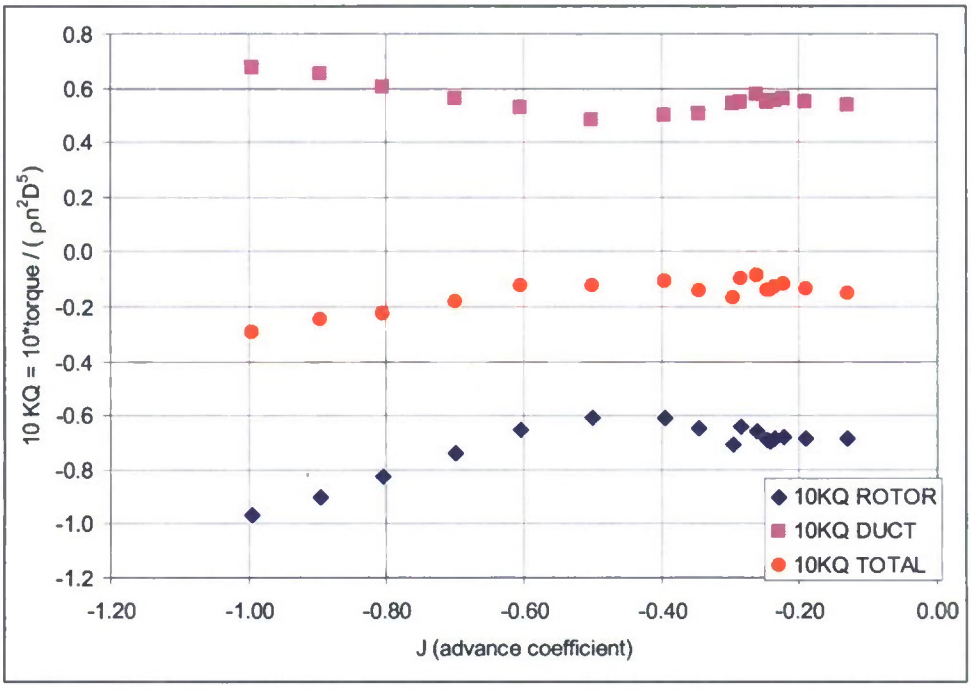


Figure 13. Propeller torque coefficient (10KQ) for rotor, duct, and combined magnitude for ducted propeller configuration under crashback conditions.

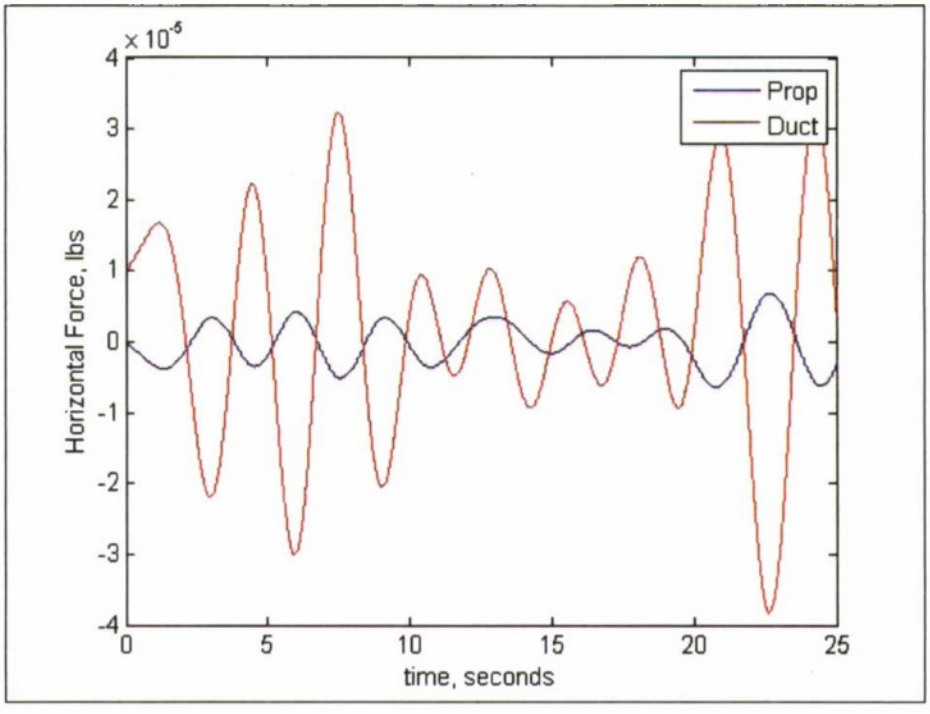


Figure 14. Horizontal force for propeller (prop) and duct for J=-0.345.

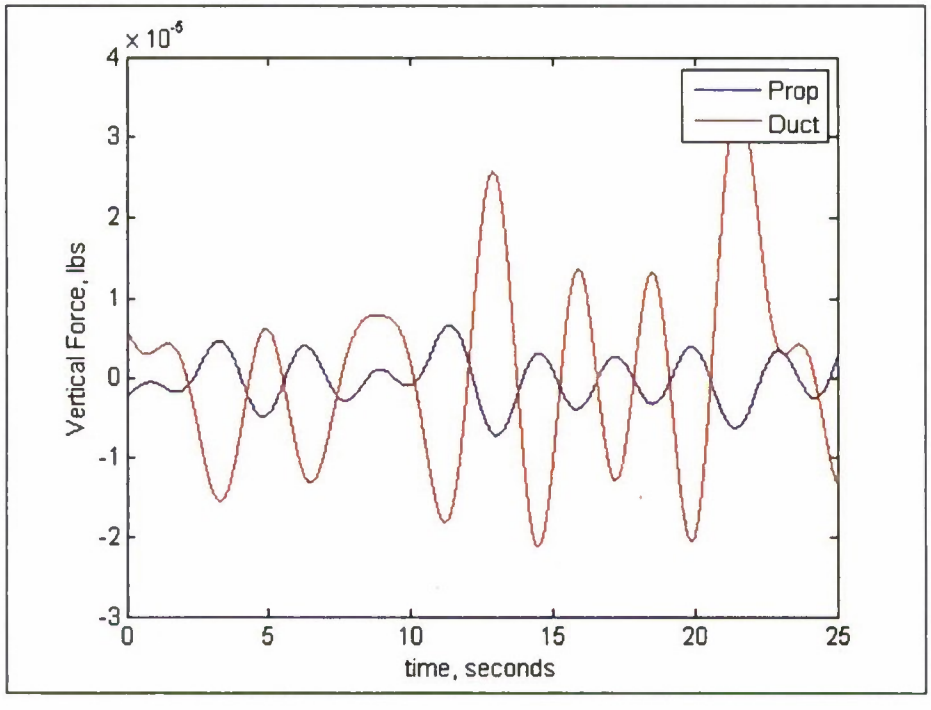


Figure 15. Vertical force for propeller (prop) and duct for J=-0.345.

For the ahead cases, propeller thrust coefficients, $K_T$, are shown in Figure 16, and torque coefficients, $K_Q$, are shown in Figure 17. Numerical predictions computed by our group are also shown on the plots. $K_T$ is dominated by the rotor contribution near the design condition (J=0.889), but the duct contribution is significantly below the design condition, and increases as J approaches zero. The numerical results for the duct contribution show a high degree of correlation with the experimental data. The rotor contribution, however, is over predicted in comparison with the experimental data, causing the total $K_T$ estimation to be high as well. Propeller torque is dominated by the rotor for all positive J values investigated. The numerical estimations again show fairly good agreement with some overestimation due to the rotor model.

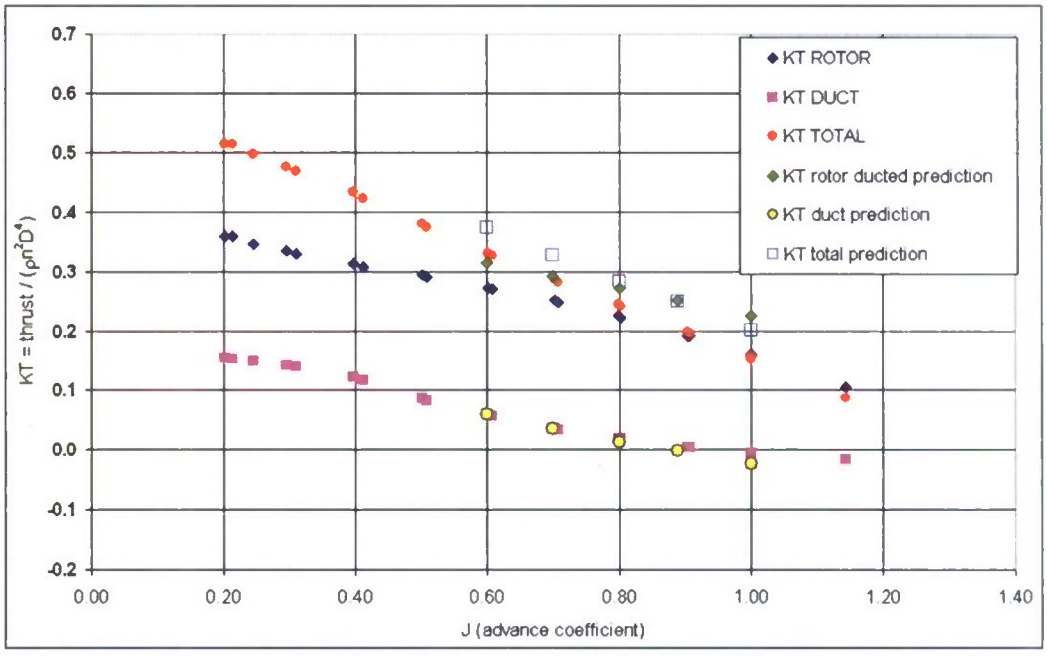


Figure 16. Propeller thrust coefficient (KT) for rotor, duct, and combined magnitude for ducted propeller configuration under ahead conditions.

Peak non-dimensional force frequencies of rotation were computed for open and ducted configurations from the phase angle of the force. The phase angle is given by the arctangent of the vertical force component divided by the horizontal component. The rotational frequencies are determined as the slope of the force angular direction versus time curve, which is indicative of a constant rotation, i.e. when the angle of the force changes linearly with time. Regression lines are computed between local extrema in the phase angle curve to determine the corresponding frequencies, and from these the maximum and minimum are taken to determine the range at which these major frequency events are occurring. Extrema are determined by low-pass filtering the raw data with an 8 Hz cutoff frequency and computing the derivative of the phase angle, theta. The troughs and peaks are then determined from the change in sign of the

derivative. Results for this process are shown in Figure 18, with the extrema locations shown as vertical lines. Regressions lines are computed between these successive locations on the raw

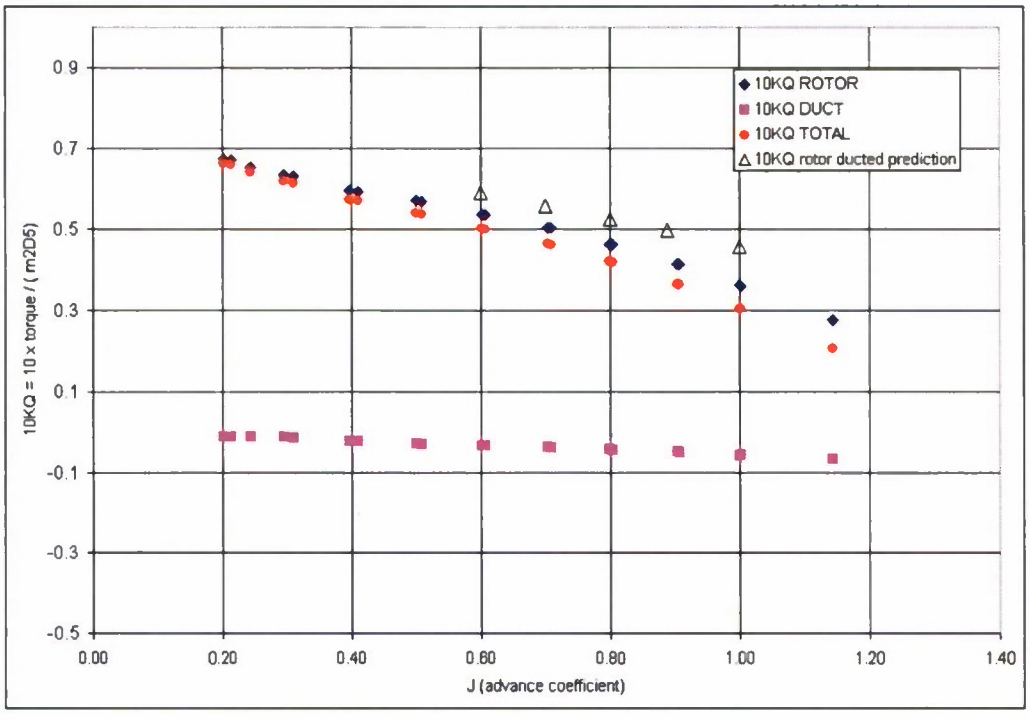


Figure 17. Propeller torque coefficient (KQ) for rotor, duct, and combined magnitude for ducted propeller configuration under ahead conditions.

data to determine the local slope, or frequency of rotation, as shown in Figure 19. Non-dimensional frequency of rotation ranges are plotted in Figure 20 with data from previous experiments. The current frequency maxima and minima (red triangles and green circles) show significant difference versus the previous experiment with an open propeller (blue squares). The duct and ducted rotor show clear agreement in range, and show an increase in the peak frequency range as J approaches -0.3.

Peak non-dimensional force frequencies of rotation were computed for open and ducted configurations from the phase angle of the force. The phase angle is given by the arctangent of the vertical force component divided by the horizontal component. The rotational frequencies are determined as the slope of the force angular direction versus time curve, which is indicative of a constant rotation, i.e. when the angle of the force changes linearly with time. Regression lines are computed between local extrema in the phase angle curve to determine the corresponding frequencies, and from these the maximum and minimum are taken to determine the range at which these major frequency events are occurring. Extrema are determined by low-pass filtering the raw data with an 8 Hz cutoff frequency and computing the derivative of the phase angle, theta. The troughs and peaks are then determined from the change in sign of the derivative. Results for this process are shown in Figure 18, with the extrema locations shown as vertical lines. Regressions lines are computed between these successive locations on the raw data to determine the local slope, or frequency of rotation, as shown in Figure 19. Non-

dimensional frequency of rotation ranges are plotted in Figure 20 with data from previous experiments. The current frequency maxima and minima (red triangles and green circles) show significant difference versus the previous experiment with an open propeller (blue squares). The duct and ducted rotor show clear agreement in range, and show an increase in the peak frequency range as J approaches -0.3.

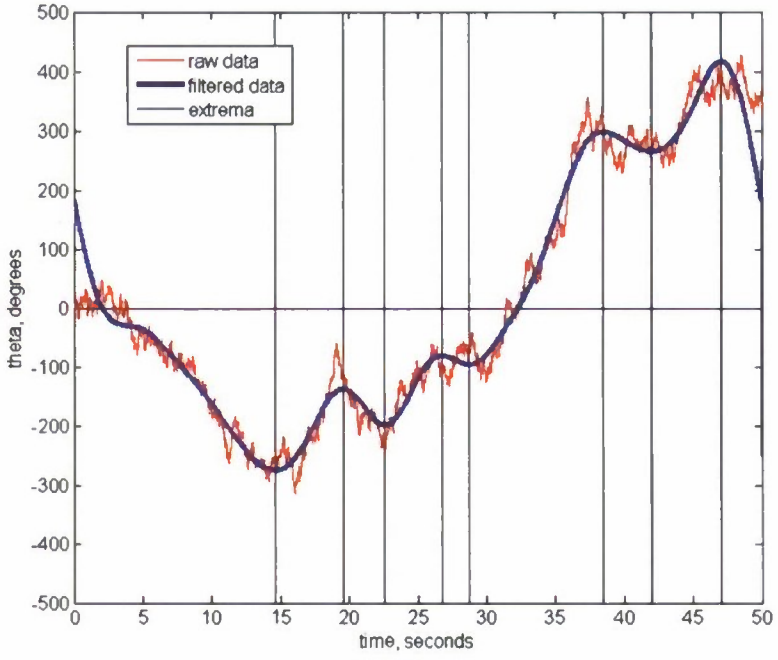


Figure 18. Raw and filtered force phase angle (theta).

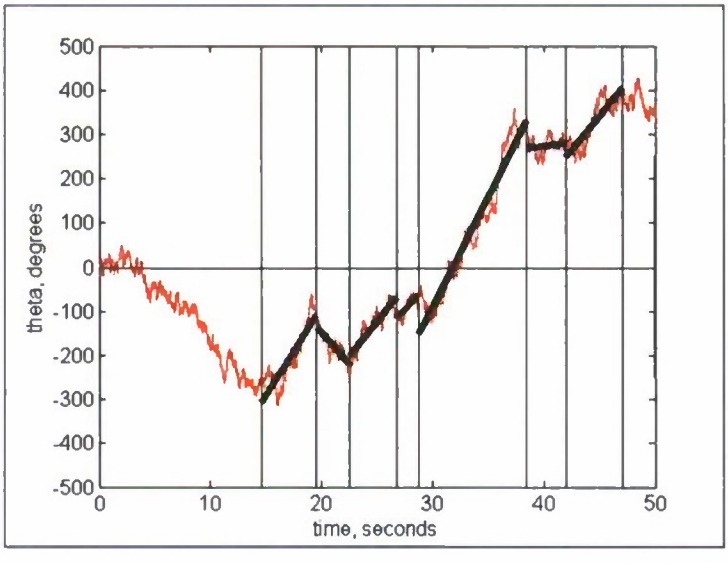


Figure 19. Linear regression lines superimposed on force phase angle (theta) versus time plot.

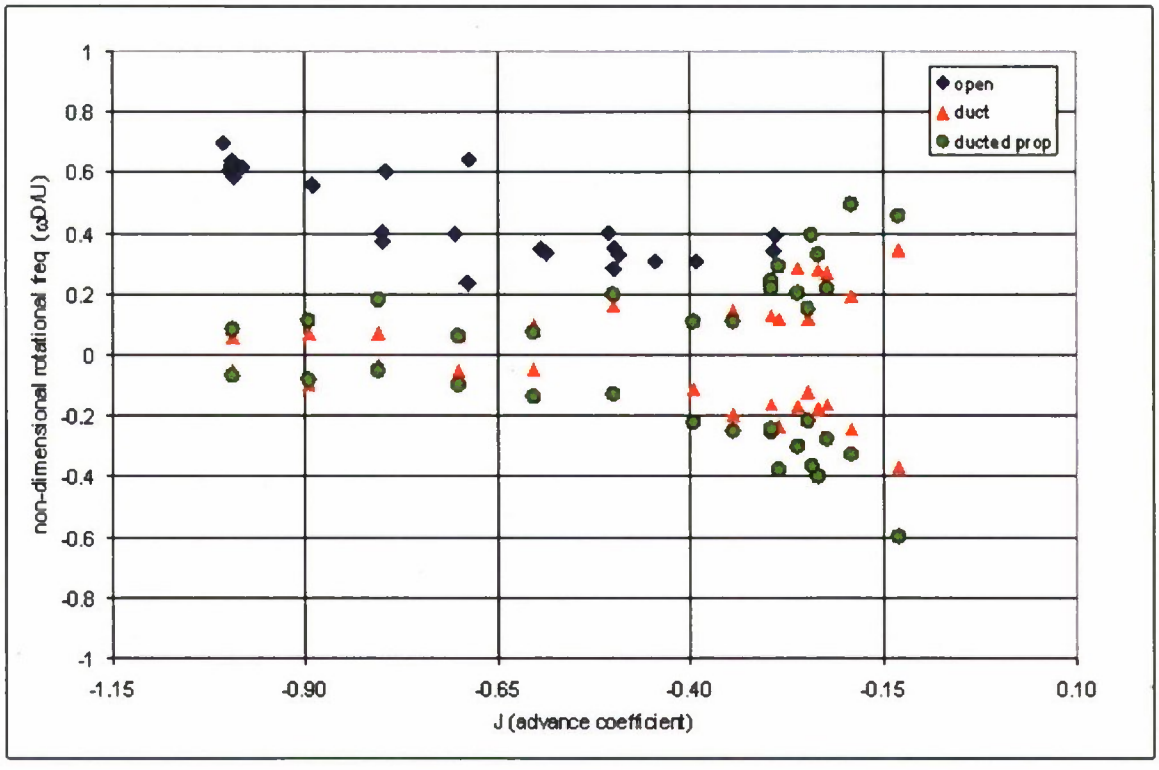


Figure 20. Non-dimensional rotational frequency (ωD/U) for ducted and open configurations.

### *Discussion of uncertainties*

Due to the rotating reference frame of the propeller, it is difficult to estimate the level of uncertainty in the measurements. In order to compare the measurement statistics between the present experiment and the previous experiment with an open rotor, normalized histograms were computed for the force magnitudes for both the rotor and duct force components. The histograms for representative J values for the crashback condition are shown in Figure 21. Good agreement is noted for the rotor histograms both with and without the duct (blue and green curves) for all J except J=-0.285. These results indicate that the experiment is repeatable. The J=-0.285 case is an extremely dynamic condition, and thus may be altered more significantly by the presence of the duct. The data presented in this fashion confirms the conclusions from Figure 10 that rotor side force magnitudes is not impacted by the presence of the duct.

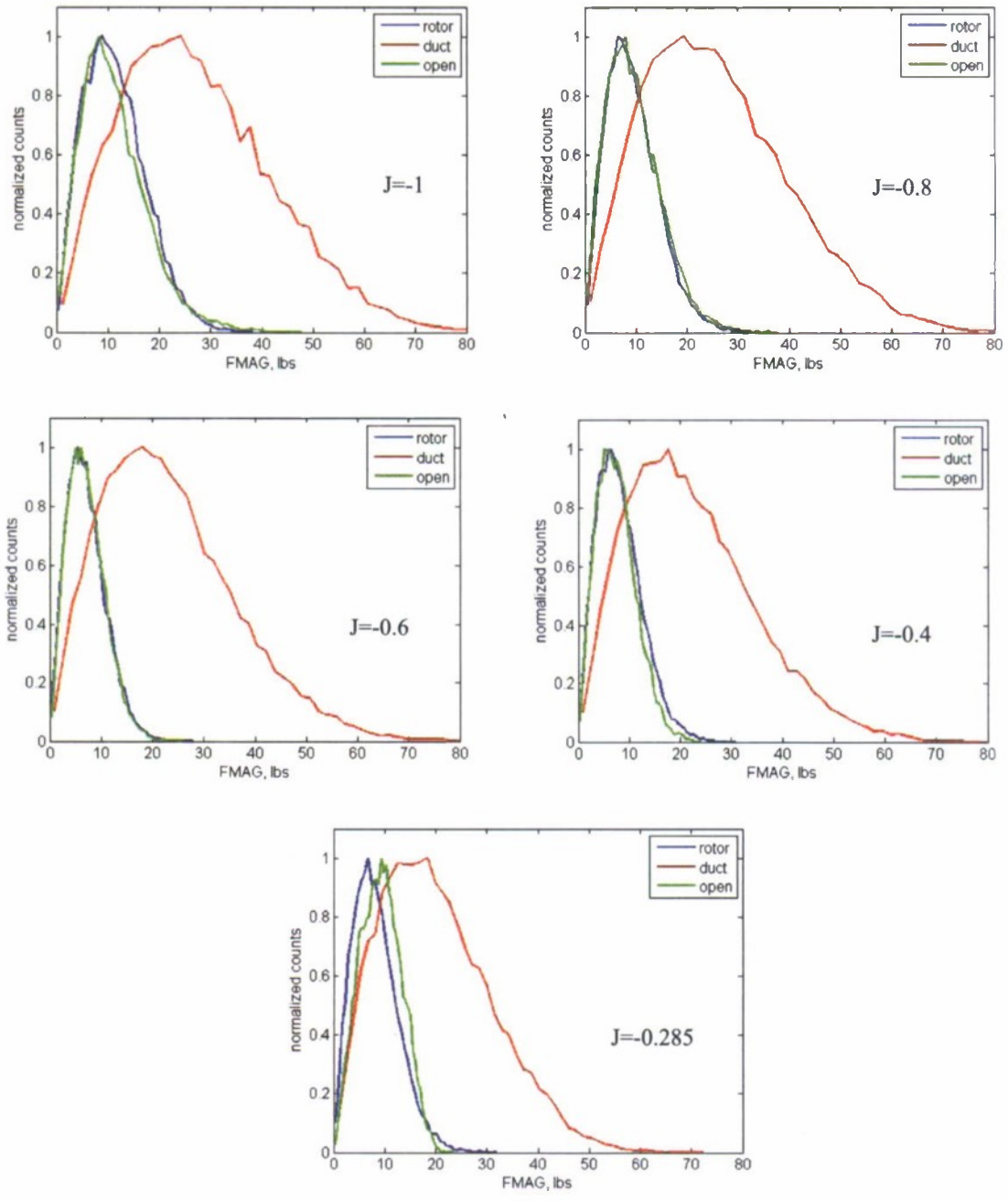


Figure 21. FMAG histograms for ducted (labeled rotor and duct) and open (labeled open) configurations.

The histograms for the open rotor configuration under all crashback conditions measured are shown in Figure 22. The force magnitude is normalized by the square root of J, as this appears to be the parameter upon which the mean and RMS are dependant. The histograms clearly collapse with some slight variation. The same results are shown in Figure 23 for the

ducted configuration, which shows significantly more spread, with the data still collapsing to some extent. Most of the variation occurs near J=-0.3, where the interaction between the duct and rotor is the greatest.

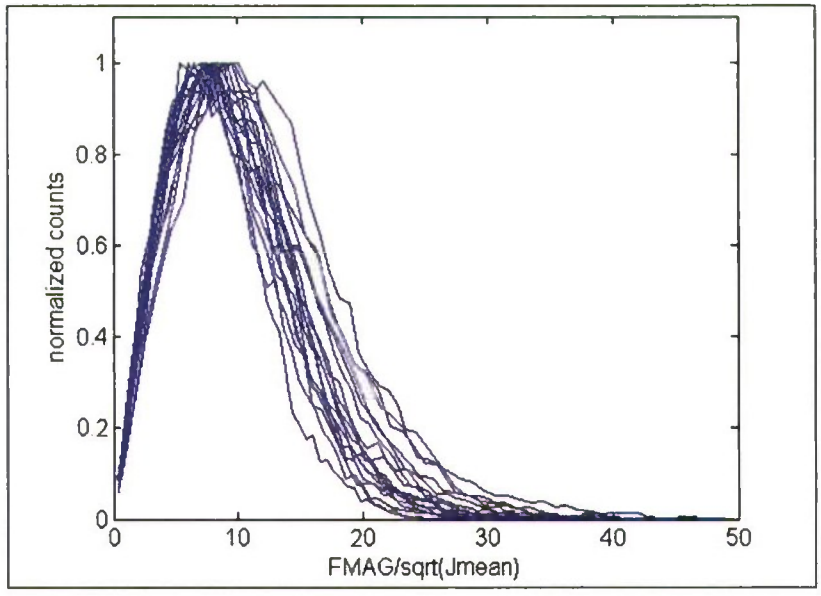


Figure 22. Rotor FMAG / sqrt(abs(J)) histograms for open propeller configuration.

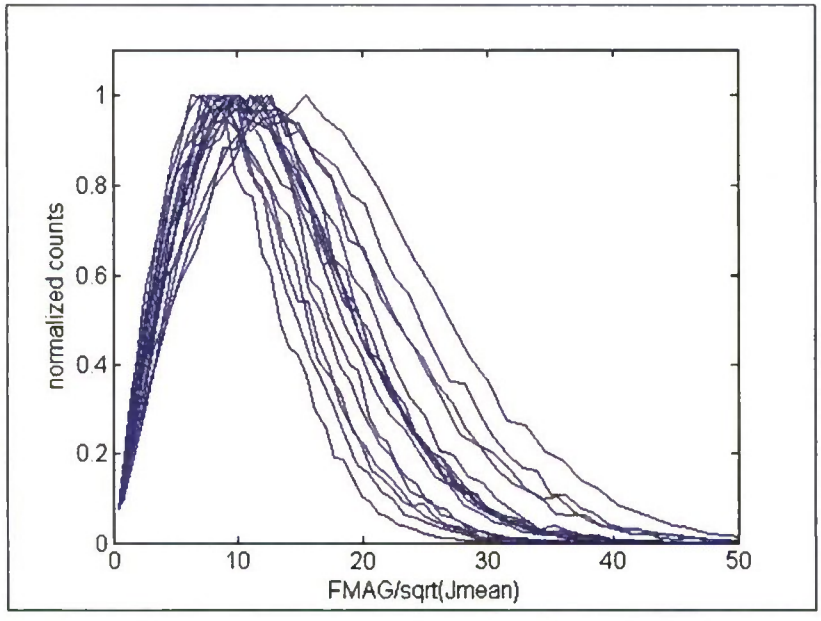


Figure 23. Rotor FMAG / sqrt(abs(J)) histograms for dueted configuration.

# CONCLUSIONS

Measurements were performed on a generic ducted propeller to determine 6-component loads in simulated crashback conditions in an open test section water tunnel. Simultaneous rotor and duct forces were measured to show the total propulsor forces. The duct forces were shown to be approximately three times the magnitude of the propeller forces. The vector sum of the rotor and stator forces were approximately similar to the duct forces with some variability due to phasing between the two propulsor components.

When comparing the unsteady side forces to the time average thrust, the rotor levels are about 10% of the propulsor thrust, while the total side force including the duct is about 30% of the rotor thrust. For this case the duct was designed as a neutral duct, producing no appreciable thrust at the ahead design condition of J=0.889. Histograms were computed for both the open and ducted configurations. These plots show the relation between the force magnitudes and the square root of the advance coefficient (J), as well as demonstrate that the experiment is repeatable. The duct has the largest apparent effect upon the rotor forces near J=-0.3, where the interaction may be non-linear.

THIS PAGE INTENTIONALLY LEFT BLANK

# APPENDIX A: Facility Characteristics

**Description of Facility**: Vertical plane, closed re-circulating with resorber, variable-speed, variable-pressure, two interchangeable circular test sections – an open jet and a closed jet, deaerator, filter system 95-micron)

**Type of Drive System**: 1.98 m (78 in) diameter adjustable pitch four-bladed axial flow impeller.

**Total Impeller Motor Power**: 2610 kW (3500 hp), 300 rpm (driving eddy current coupling)

**Total Input Power to the Pump**: 2153 kW (2887 hp), 272 rpm

**Working Section Max Velocity**: 25.7 m/s (84.5 ft/s, 50 knots)

**Max. & Min. Abs. Pressures**: 414 kPa (60 psia), 14 kPa (2 psia)

**Min. Cavitation Number**: sigma = 0.034 (at 2 psia, 50 knots)

THIS PAGE INTENTIONALLY LEFT BLANK

# APPENDIX B: Model Characteristics

## Propeller 4381

Geometric Characteristics
Number of Blades: 5
Diameter: 305 mm (12.0 Inches)
Thickness Section: NACA 66 (DTMB Modified)
Camber Section: a=0.9 meanline
Skew, Rake =0.0

| r/R | C/D | T/C | P/D | F/C |
|---|---|---|---|---|
| 0.20 | 0.174 | 0.250 | 1.26 | 0.0312 |
| 0.30 | 0.228 | 0.156 | 1.35 | 0.0369 |
| 0.40 | 0.275 | 0.107 | 1.36 | 0.0348 |
| 0.50 | 0.313 | 0.077 | 1.34 | 0.0307 |
| 0.60 | 0.338 | 0.057 | 1.28 | 0.0244 |
| 0.70 | 0.348 | 0.042 | 1.21 | 0.0189 |
| 0.80 | 0.334 | 0.031 | 1.14 | 0.0147 |
| 0.90 | 0.281 | 0.024 | 1.07 | 0.0122 |
| 0.95 | 0.219 | 0.026 | 1.03 | 0.0133 |
| 0.98 | 0.153 | 0.037 | 1.01 | 0.0164 |
| 0.99 | 0.115 | 0.050 | 1.01 | 0.0211 |
| 1.00 | 0.000 | 0.070 | 1.00 | 0.0280 |

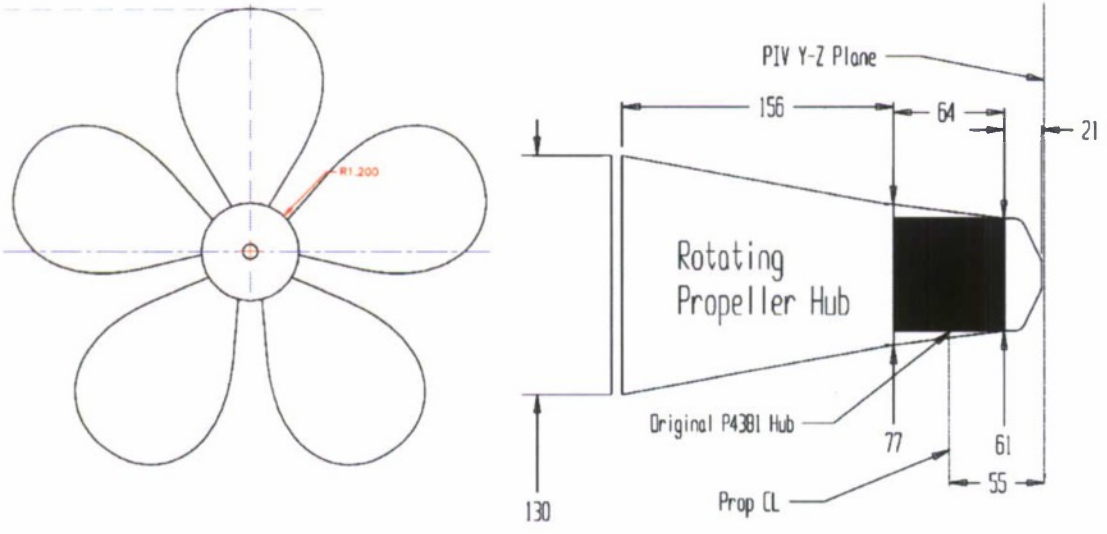

**Neutrally loaded duct**

Duct Offsets

| x (mm) | R (mm) upper | R (mm) lower |
|---|---|---|
| -156.2 | 172.4 | 172.4 |
| -152.4 | 176.4 | 168.6 |
| -139.7 | 179.0 | 165.2 |
| -127.0 | 179.6 | 163.4 |
| -114.3 | 179.6 | 162.2 |
| -101.6 | 179.2 | 161.1 |
| -88.9 | 178.5 | 160.0 |
| -76.2 | 177.7 | 159.1 |
| -63.5 | 176.8 | 158.2 |
| -50.8 | 175.9 | 157.4 |
| -38.1 | 175.0 | 156.6 |
| -25.4 | 174.1 | 155.9 |
| -1.3 | 173.3 | 155.2 |
| 0.0 | 172.5 | 154.6 |
| 12.7 | 171.7 | 154.1 |
| 25.4 | 170.7 | 153.6 |
| 38.1 | 169.4 | 153.2 |
| 50.8 | 167.6 | 152.9 |
| 63.5 | 165.1 | 152.7 |
| 76.2 | 162.0 | 152.5 |
| 88.9 | 158.2 | 152.4 |
| 98.9 | 153.2 | 153.2 |

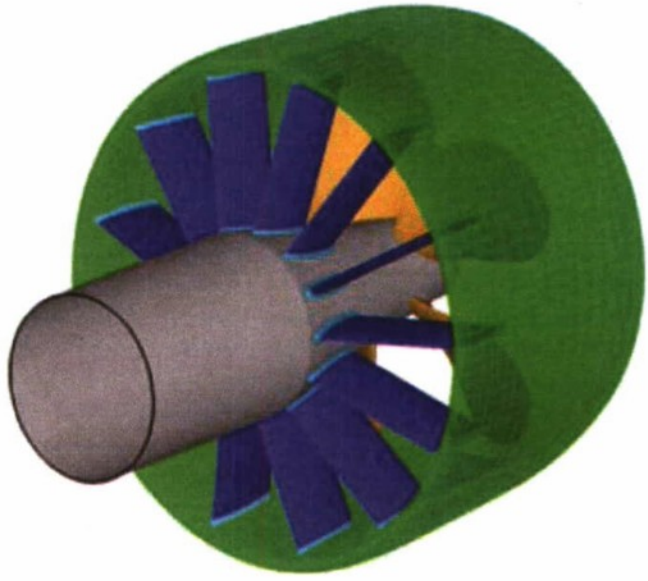

# APPENDIX C: Ducted configuration assembly drawing

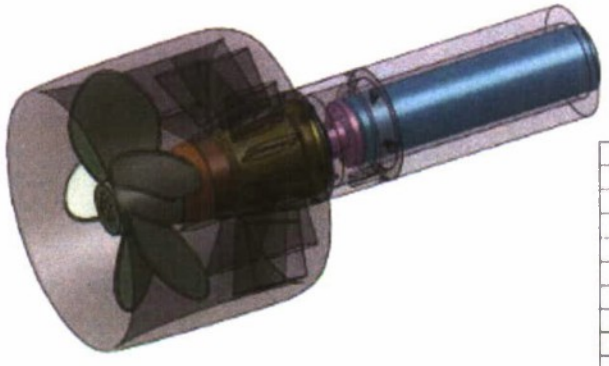

| ITEM NO. | DESCRIPTION | QTY. |
|---|---|---|
| 1 | Crashback dyno | 1 |
| 2 | Tunnel and Stator Tube | 1 |
| 3 | Stator Tube Spacer | 1 |
| 4 | Stator Hub | 1 |
| 5 | Tunnel Rotor Shaft | 1 |
| 6 | Rotor Dyno | 1 |
| 7 | Prop Hub | 1 |
| 8 | Rotor Flange | 1 |
| 9 | Rotor Shaft | 1 |
| 10 | Stator | 1 |

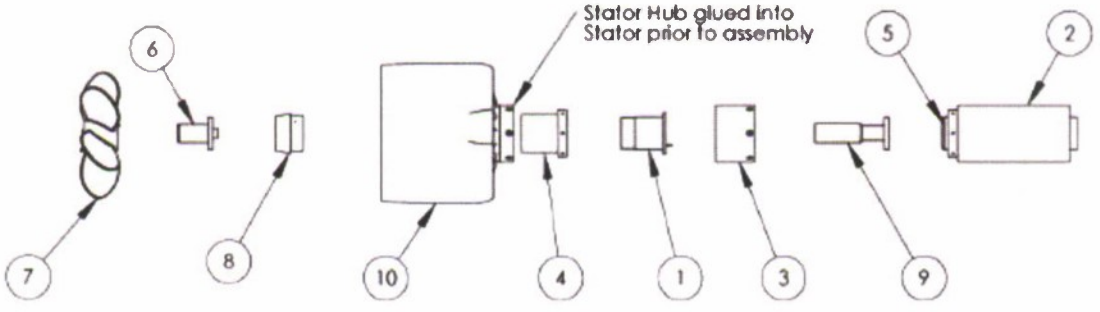


Figure C1: Ducted configuration assembly drawing.

THIS PAGE INTENTIONALLY LEFT BLANK

# APPENDIX D: Propeller Dynamometer Drawing

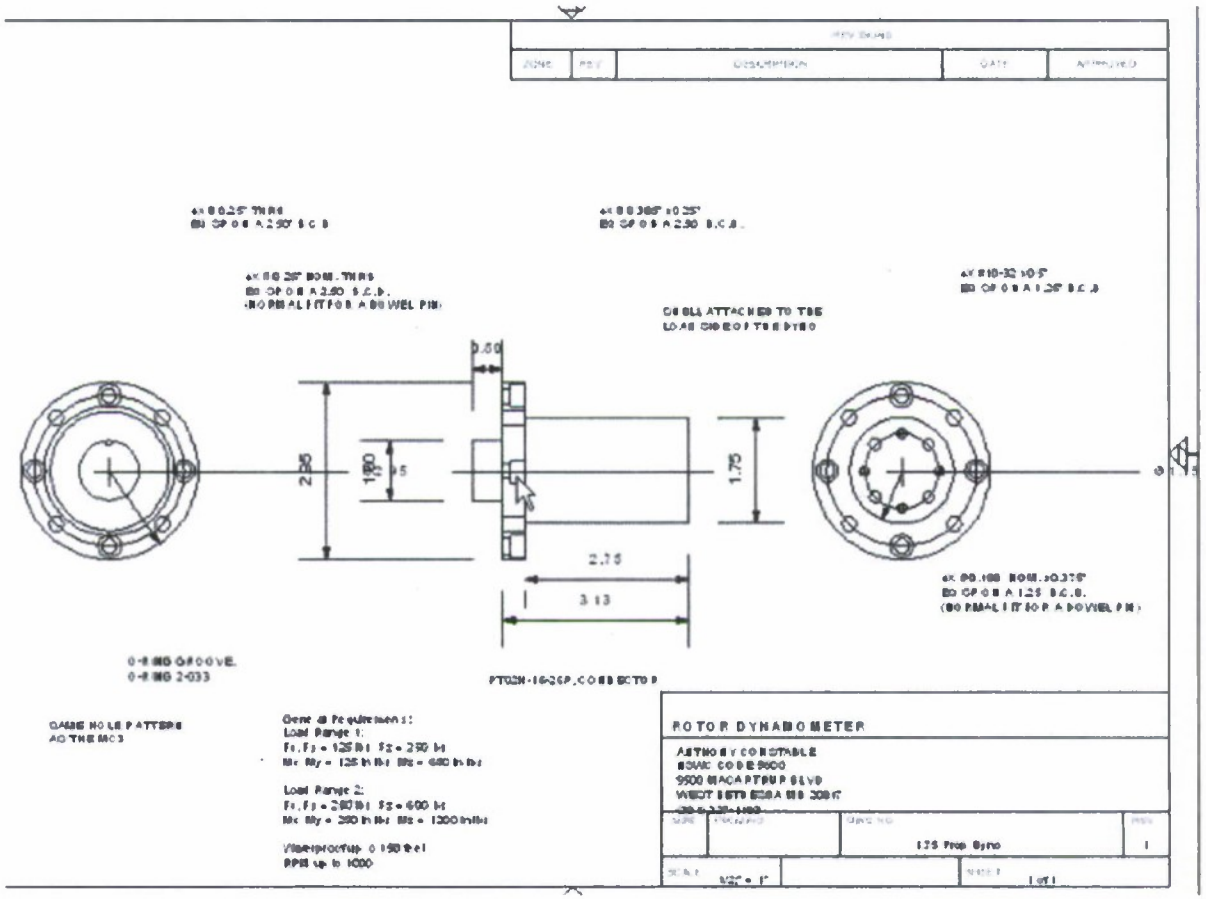


Figure D1: Propeller dynamometer drawing.

THIS PAGE INTENTIONALLY LEFT BLANK

# APPENDIX E: Stator Dynamometer Drawing

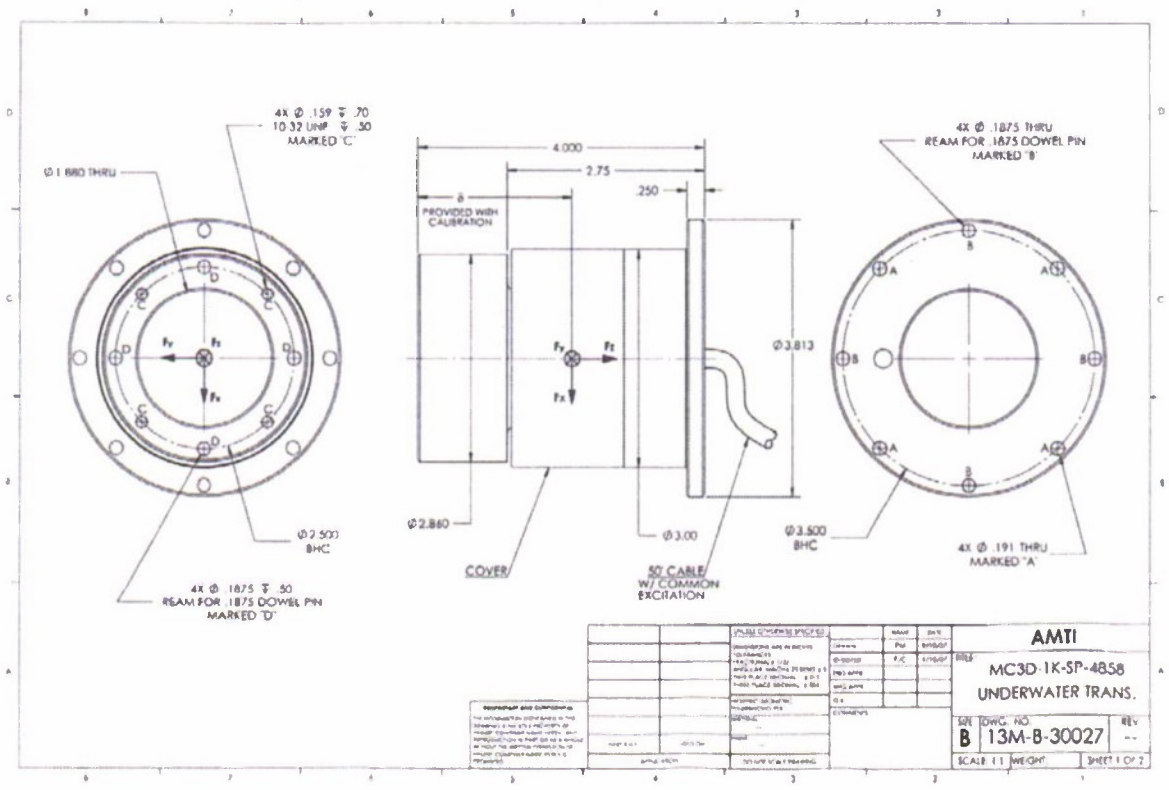


Figure E1: Stator dynamometer drawing

THIS PAGE INTENTIONALLY LEFT BLANK

# APPENDIX F: Rotor and stator dynamometer calibrations

**Calibration Report - AMTI STOCK - 36" WT ROTOR - M4235** **DATE: 01302008**

| | | | | | | | | | | | | |
|---|---|---|---|---|---|---|---|---|---|---|---|---|
| Xducer Info: | | | | | | | | | | | | |
| Xducer Type: | AMTI STOCK | Xducer Name: | 36" WT ROTOR | Xducer FUnits: | LBS | Xducer MUnits: | IN-LBS | Serial #: | M4235 | Barcode #: | | Xducer Cap: | 0 |
| Ref Info: | | | | | | | | | | | | | |
| Ref Type: | NONE | Ref Units: | | Ref Gain: | | Ref Zero: | | Ref Cal Due: | | | | | |
| Sig Cond Info: | | | | | | | | | | | | | |
| SCType: | NONE | SCBarcode: | | SCSerNum: | | Gain: | 0 | Gain Pot: | 0 | LP Filter: | 1 KHz | | |
| Span Info: | | | | | | | | | | | | | |
| Pos Cal: | 0 | Neg Cal: | 0 | Exp Span: | 0 | | | | | | | | |
| FootprintSize: | 4" Block gage | | | | | | | | | | | | |
| DAQ Info: | | | | | | | | | | | | | |
| DAQType: | PXI-6031E DAQ S | 17109349 | Counts/Volt: | 6553.6 | | | | | | | | | |
| ChNames: | Fx | Fy | Fz | Mx | My | Mz | | | | | | | |
| ChNums: | 0 | 1 | 2 | 3 | 4 | 5 | | | | | | | |
| Cal Stand Info: | | | | | | | | | | | | | |
| Multipliers: | 1 | 1 | 1 | 1 | 1 | 1 | | | | | | | |
| Stand Type: | Fixed | Cal Type: | Autonomous Model | | | | | | | | | | |
| Moment Arm Matrix | | | | | | | | | | | | | |
| 1 | 0 | 0 | 0 | 0 | 0 | | | | | | | | |
| 0 | 1 | 0 | 0 | 0 | 0 | | | | | | | | |
| 0 | 0 | 1 | 0 | 0 | 0 | | | | | | | | |
| 0 | 0 | 0 | 1 | 0 | 0 | | | | | | | | |
| 0 | 0 | 0 | 0 | 1 | 0 | | | | | | | | |
| 0 | 0 | 0 | 0 | 0 | 1 | | | | | | | | |
| XducerComment: | FOR 36" WATERTUNNEL CRASHBACK EXPERIMENT '08 | | | | | | | | | | | | |

| Axis: | -Fx | -Mz | -Fx | +My | -Fx | +Fy | +Mx | +Fx | -My | -Fy | -Mx | -Mz |
|---|---|---|---|---|---|---|---|---|---|---|---|---|
| A0(Zero): | -0.00161842 | -0.00297391 | -0.00823356 | -0.00007497 | 0.0001351 | 0.00286622 | 0.0026308 | 0.0055999 | -0.001302 | -0.005431 | -0.004855 | 0.0001603 |
| A1(Sensitivity): | 0.08741364 | 0.0142723 | 0.06751506 | 0.02168754 | 0.0675314 | 0.06704022 | 0.0217818 | 0.0675066 | 0.0217306 | 0.066987 | 0.0217688 | 0.0142692 |
| IOD (R^2): | 0.99999529 | 0.99998288 | 0.99999541 | 0.99999757 | 0.9999985 | 0.99999385 | 0.9999956 | 0.9999952 | 0.9999881 | 0.9999945 | 0.9999961 | 0.9999929 |
| STEYX(V): | 0.00545329 | 0.01036709 | 0.00539206 | 0.00298891 | 0.0031267 | 0.00619467 | 0.0040236 | 0.0054928 | 0.0066206 | 0.0058667 | 0.0038268 | 0.0067504 |
| STEYX(EU): | 0.06069303 | 0.72837795 | 0.07986448 | 0.13781686 | 0.0463297 | 0.09240234 | 0.1847224 | 0.0813673 | 0.304665 | 0.0875794 | 0.1757927 | 0.4730725 |
| Correlation Coef | -0.99999765 | -0.99999144 | -0.99999771 | -0.99999879 | 0.9999992 | 0.99999693 | 0.9999978 | 0.9999978 | -0.999994 | -0.999997 | -0.999998 | 0.9999964 |
| Gain(EU/V): | 14.83379249 | 70.06577279 | 14.81150921 | 46.10943448 | 14.807934 | 14.9164186 | 45.909975 | 14.813372 | 46.018034 | 14.92826 | 45.937282 | 70.081165 |
| Offset(EU): | 0.02397789 | 0.2063695 | 0.09232823 | 0.00345697 | -0.002001 | -0.0427538 | -0.12078 | -0.082954 | 0.0599285 | 0.0810723 | 0.2230419 | -0.011232 |

| Gains | IM | | | | | | Gains | Norm | | | | |
|---|---|---|---|---|---|---|---|---|---|---|---|---|
| 1 | 14.802029 | 0.039519 | -0.254498 | 0.015996 | 0.436801 | 0.056616 | 14.802029 | 1 | 0.00267 | -0.017193 | 0.001081 | 0.029502 | 0.003825 |
| 1 | -0.211433 | 14.905957 | 0.150372 | -0.438014 | -0.019383 | -0.086737 | 14.905957 | -0.014184 | 1 | 0.010088 | -0.029385 | -0.0013 | -0.005819 |
| 1 | -0.000005 | -0.021138 | 28.877353 | -0.483223 | -0.043961 | 0.16384 | 28.877353 | 0 | -0.000732 | 1 | -0.016734 | -0.001522 | 0.005674 |
| 1 | 0.113834 | -0.153708 | 0.395181 | 45.834624 | 0.284427 | -0.069747 | 45.834624 | 0.002484 | -0.003354 | 0.008622 | 1 | 0.006206 | -0.001522 |
| 1 | 0.105414 | 0.071243 | 1.204086 | -0.535238 | 46.071499 | -0.109126 | 46.071499 | 0.002288 | 0.001546 | 0.026135 | -0.011818 | 1 | -0.002369 |
| 1 | -0.275247 | -0.314913 | -0.565654 | 0.04943 | 0.101676 | 69.899712 | 69.899712 | -0.003938 | -0.004505 | -0.008092 | 0.000707 | 0.001455 | 1 |

| Metrics: | | | | | | |
|---|---|---|---|---|---|---|
| MaxRange | 100 | 100 | 250 | 250 | 250 | 500 |
| ErrMax | 0.159945 | 0.386956 | 3.01262 | 11.767582 | 0.751621 | 0.752621 |
| ErrMin | -0.147552 | -0.126226 | -0.510536 | -4.439017 | -0.431331 | -1.684535 |
| ErrStDev | 0.067647 | 0.087707 | 0.644043 | 1.490348 | 0.21348 | 0.425064 |
| %ErrMax | 0.159945 | 0.386956 | 1.205048 | 4.715033 | 0.300648 | 0.150524 |
| %ErrMin | -0.147552 | -0.126226 | -0.204215 | -1.775607 | -0.172532 | -0.336907 |
| %ErrStDev | 0.067647 | 0.087707 | 0.257617 | 0.596139 | 0.085392 | 0.085013 |

Table F1: Rotor dynamometer calibration

**Calibration Report - AMTI STOCK - 36" WT STATOR - M4812** **DATE: 01162008**

| | | | | | | | | | | | | | |
|---|---|---|---|---|---|---|---|---|---|---|---|---|---|
| Xducer Info: | | | | | | | | | | | | | |
| Xducer Type: | AMTI STOCK | Xducer Name: | 36" WT STATOR | Xducer FUnits: | LBS | Xducer MUnits: | IN-LBS | Serial #: | M4812 | Barcode #: | | Xducer Capacity: | 0 |
| Ref Info: | | | | | | | | | | | | | |
| Ref Type: | NONE | Ref Units: | | Ref Gain: | | Ref Zero: | | Ref Cal Due: | | | | | |
| Sig Cond Info: | | | | | | | | | | | | | |
| SCType: | NONE | SCBarcode: | | SCSerNum: | | Gain: | 0 | Gain Pot: | 0 | LP Filter: | 1 KHz | | |
| Span Info: | | | | | | | | | | | | | |
| Pos Cal: | 0 | Neg Cal: | 0 | Exp Span: | 0 | | | | | | | | |
| FootprintSize: | 4" Block gage | | | | | | | | | | | | |
| DAQ Info: | | | | | | | | | | | | | |
| DAQType: | PXI-6031E DAQ SN | 17109349 | Counts/Volt: | 6553.6 | | | | | | | | | |
| ChNames: | Fx | Fy | Fz | Mx | My | Mz | | | | | | | |
| ChNums: | 0 | 1 | 2 | 3 | 4 | 5 | | | | | | | |
| Cal Stand Info: | | | | | | | | | | | | | |
| Multipliers: | 1 | 1 | 1 | 1 | 1 | 1 | | | | | | | |
| Stand Type: | Fixed | Cal Type: | Autonomous Model | | | | | | | | | | |
| Moment Arm Matrix | | | | | | | | | | | | | |
| 1 | 0 | 0 | 0 | 0 | 0 | | | | | | | | |
| 0 | 1 | 0 | 0 | 0 | 0 | | | | | | | | |
| 0 | 0 | 1 | 0 | 0 | 0 | | | | | | | | |
| 0 | 0 | 0 | 1 | 0 | 0 | | | | | | | | |
| 0 | 0 | 0 | 0 | 1 | 0 | | | | | | | | |
| 0 | 0 | 0 | 0 | 0 | 1 | | | | | | | | |
| XducerComment: | FOR 36" WATERTUNNEL CRASHBACK EXPERIMENT '08 | | | | | | | | | | | | |

| Axis: | -Mz | +Mz | +Fy | +Mx | -Fx | +My | +Fx | -My | -Fy | -Mx | -Mx | +Fz |
|---|---|---|---|---|---|---|---|---|---|---|---|---|
| A0(Zero): | -0.00169376 | 0.00264936 | 0.00131773 | 0.00172939 | -0.002017 | 0.00144488 | 0.00148759 | -0.001139 | -0.00174 | -0.001576 | -0.001576 | 0.00135995 |
| A1(Sensitivity): | 0.00973355 | 0.00973548 | 0.03681245 | 0.01942076 | 0.0367988 | 0.01951915 | 0.03680801 | 0.0195105 | 0.0368031 | 0.019423 | 0.019423 | 0.01804802 |
| IOD (R^2): | 0.99999823 | 0.99999768 | 0.99999937 | 0.9999989 | 0.9999992 | 0.99999836 | 0.99999891 | 0.9999986 | 0.9999986 | 0.9999979 | 0.9999979 | 0.99999852 |
| STEYX(V): | 0.00150713 | 0.00262711 | 0.00109116 | 0.00180327 | 0.0011997 | 0.00221112 | 0.0014348 | 0.0020435 | 0.0016389 | 0.0024794 | 0.0024794 | 0.00194173 |
| STEYX(EU): | 0.15483839 | 0.26984955 | 0.02964115 | 0.09285267 | 0.0326005 | 0.11327935 | 0.03898068 | 0.1047362 | 0.0445318 | 0.1276532 | 0.1276532 | 0.10758679 |
| Correlation Coeffi | -0.99999962 | 0.99999884 | 0.99999968 | 0.99999945 | -1 | 0.99999916 | 0.99999945 | -0.999999 | -0.999999 | -0.999999 | -0.999999 | 0.99999926 |
| Gain(EU/V): | 102.7374562 | 102.7171153 | 27.18472579 | 51.49128387 | 27.174809 | 51.23175125 | 27.1679995 | 51.254544 | 27.171625 | 51.485312 | 51.485312 | 55.4077492 |
| Offset(EU): | 0.17401271 | -0.27213472 | -0.03579575 | -0.08904826 | 0.0548067 | -0.07402353 | -0.0404149 | 0.0583917 | 0.0472653 | 0.0811431 | 0.0811431 | -0.07535154 |

| Gains | IM | | | | | | Gains | Norm | | | | |
|---|---|---|---|---|---|---|---|---|---|---|---|---|
| 1 | 27.145063 | 0.516777 | 0.077416 | 0.577233 | -0.401824 | -0.051688 | 27.145063 | 1 | 0.019038 | 0.002852 | 0.021265 | -0.014803 | -0.001904 |
| 1 | 0.002873 | 27.149286 | -0.114503 | 0.425937 | 0.206627 | 0.016921 | 27.149286 | 0.000106 | 1 | -0.004218 | 0.015689 | 0.007611 | 0.000623 |
| 1 | -0.203842 | 0.199054 | 55.36088 | 0.285679 | 0.176291 | -0.032385 | 55.36088 | -0.003682 | 0.003596 | 1 | 0.00516 | 0.003184 | -0.000585 |
| 1 | -0.513214 | -0.152743 | 0.081064 | 51.446111 | 1.113558 | -0.068269 | 51.446111 | -0.009976 | -0.002969 | 0.001576 | 1 | 0.021645 | -0.001327 |
| 1 | 0.120946 | 0.382934 | 0.077084 | 0.275187 | 51.225356 | -0.024822 | 51.225356 | 0.002361 | 0.007475 | 0.001505 | 0.005372 | 1 | -0.000485 |
| 1 | 0.200261 | -0.09117 | -1.313943 | -0.244097 | 0.509074 | 102.653852 | 102.653852 | 0.001951 | -0.000888 | -0.0126 | -0.002378 | 0.004959 | 1 |

| Metrics: | | | | | | |
|---|---|---|---|---|---|---|
| MaxRange | 100 | 100 | 250 | 250 | 250 | 500 |
| ErrMax | 0.090927 | 0.167816 | 0.620748 | 0.316522 | 0.48883 | 0.975824 |
| ErrMin | -0.299924 | -0.142469 | -0.251167 | -0.160799 | -0.18838 | -0.988916 |
| ErrStDev | 0.054377 | 0.056659 | 0.134062 | 0.096258 | 0.105416 | 0.260869 |
| %ErrMax | 0.090927 | 0.167816 | 0.248299 | 0.126609 | 0.195532 | 0.195165 |
| %ErrMin | -0.299924 | -0.142469 | -0.100475 | -0.06432 | -0.075352 | -0.197784 |
| %ErrStDev | 0.054377 | 0.056659 | 0.053625 | 0.038503 | 0.042166 | 0.052174 |

Table F2: Rotor dynamometer calibration

## ACKNOWLEDGMENTS

The work deseribed in this report could not have been done without the hard work and dedieation of Mr. David Boehinski, Mr. David J. Grant, and Ms. Nikia Mast. Their effort and expertise are mueh appreeiated.

THIS PAGE INTENTIONALLY LEFT BLANK

## REFERENCES


1. Jiang, C.W., Dong, R.R., Liu, H.L. and Chang, M.S., "24-inch Water Tunnel flow Field Measurements During Propeller Crashback," 21st ONR Symposium on Naval Hydrodynamics, 1996, Trondheim, Norway, pp. 136-146.
2. Jessup, S., Fry, D., and Donnelly, M., "Unsteady Propeller Performance in Crashback Condition With and Without a Duct," 26th Symposium on Naval Hydrodynamics, Rome, Italy 17-22 September, 2006.
3. Chen, B., , "Computational Fluid Dynamics of Four-Quadrant Marine Propeller Flow", Ms.Sc. Thesis, The University of Iowa. 1996.
4. Davoudzadeh, F., et. al., " Coupled Navier-Stokes and Equations of Motion Simulation of Submarine Maneuvers, Including Crashback," ASME Fluids Engineering Division Summer Meeting, Vancouver, British Columbia, Canada, 1997.
5. Vysohlid, M., Mahesh, K., "Large Eddy Simulation of Crashback in Marine Propellers," AIAA Paper 2006-1415.
6. Vysohlid, M. and Mahesh, K., "Understanding Crashback in Marine Propellers Using an Unsteady Actuator Disk Model," 45th AIAA Paper 2007-918.
7. Bridges, D. H., Donnelly, M. J., and Park, J. T., "Experimental Investigation of the Submarine Crashback Maneuver," Journal of Fluids Engineering, vol. 130, January 2008, pp. 011103-1 to 011103-11.
8. Chesnakas, C., Donnelly, M., Fry, D., Jessup, S., and Park, J., "Performance of Propeller 4381 in Crashback," NSWCCD-50-TR-2004/010 December 2004.

THIS PAGE INTENTIONALLY LEFT BLANK

## INITIAL DISTRIBUTION

| Copies | | Code | Name | Center Distribution Copies | Code | Name |
|---|---|---|---|---|---|---|
| 3 | ONR | | | 1 | 3452 | Library (pdf) |
| | 1 | 333 | Joslin | 1 | 5030 | Jessup |
| | 1 | 333 | Kim | 1 | 5060 | Walden |
| | 1 | 333 | Purtell | 1 | 5080 | Brown |
| | | | | 1 | 5600 | Bochinski |
| | 1 | 333 | DTIC | 1 | 5600 | Junghans |
| | | | | 1 | 5600 | Lee |
| | | | | 1 | 5600 | Lewis |
| | | | | 2 | 5800 | Files |
| | | | | 1 | 5800 | Hurwitz (pdf) |